

Statistical model analysis of multiparticle correlations in e^+e^- annihilation

T.Osada^{*†}, M.Maruyama, F.Takagi

Department of Physics, Tohoku University, Sendai 980-8578, Japan

July 12, 2021

Abstract

A new statistical model for multiparticle production in e^+e^- annihilation is proposed based on the idea of the longitudinal phase space with limited transverse momentum. The longitudinal rapidity space is divided into cells of equal size in order to take into account the Bose-Einstein correlations(BEC) with a finite correlation length δy . The maximum entropy method is used to determine the probability distributions of the final state pions (or ρ mesons) for a given mean multiplicity, mean transverse momentum and mean total energy. Event simulation based on our model is performed in two extreme cases, a π -model and a ρ -model. The π -model assumes that only pions are produced directly. On the other hand, the ρ -model assumes that only ρ mesons are produced directly and they decay into pions. A good overall fit to experimental data from PETRA to LEP energy regions is obtained for δy ranging from 0.6 to 1.2 in the π -model. We found that the BEC plays a very important role to reproduce various correlation data. In some correlation data, resonance effect and conservation laws are also important.

PACS: 12.40.Ee, 13.65.+i, 02.70.Lq, 05.40.+j, 25.75.Gz.

1 Introduction

With increase in energies of accelerators, accurate data on high-multiplicity events at high energies have recently been provided. This makes it possible to analyze correlations and fluctuations such as the Bose-Einstein correlations (BEC)[1] and the intermittency [2, 3] in detail. These correlations and fluctuations of produced particles are rather new tools to study multiparticle production. By analyzing them, one may be able to extract useful information on the space-time size of the particle production region and the production mechanism[1]. Correlations and fluctuations may also provide a clear signal of quark gluon plasma formation expected in high energy nucleus-nucleus collisions. On the other hand, multiparticle production is a phenomenon observed commonly in various reactions such as

^{*}e-mail address: osada@nucl.phys.tohoku.ac.jp

[†]Address after June 1998: *Instituto de Física, Universidade de São Paulo, C.P.66318, 05389-470 São Paulo-SP, Brazil*

e^+e^- annihilations, lepton-hadron deep inelastic interactions, hadron-hadron interactions, and nucleus-nucleus collisions. A large amount of correlation data has been accumulated on various reactions. It has been found that there are some universal characteristics which are independent of the reaction type while some other properties depend on it. Phenomenological models which can describe some crucial properties of many particle correlations will be very useful for systematic investigations of those characteristics caused by correlations and fluctuations.

The BEC have lately attracted considerable attention, in particular, because they may give information on the space time structure of hadronic source and they may cause large fluctuations of particle density in the phase space. Although many existing phenomenological models have not taken into account the BEC completely yet, there are some models (or event generators) which allow computing the two identical particle correlation functions. In most cases, the BEC are generated more or less artificially. For example, they are calculated by using (i) the Fourier transformation of the model's source function[4] or (ii) the Wigner function[5], (iii) by weighting every event[6], or (iv) by modifying the distribution of momentum difference of identical particle pairs in each event[7]. However, some of those models cannot describe the BEC in a single event. Motivated by those consideration, we would like to propose a new statistical model. It is constructed by the maximum entropy method [8, 9] and two versions of the model, the π -model and the ρ -model are applied to e^+e^- annihilation in this paper. The most characteristic point of our model is that the BEC is taken into account in quantum statistical level with a characteristic correlation length (δy) defined in the rapidity space.

This paper is organized as follows. In Sec.II, our model is explained and the distribution functions of the final state hadrons are derived. Sec.III is devoted to the explanation of the simulation method including the procedure of parameter determination. Comparison of results obtained from simulation with the experimental data from PETRA to LEP energies is given in Sec.IV. Concluding remarks and discussions are given in Sec.V.

2 Statistical model based on Maximum Entropy Method

We first consider the π -model, i.e., we assume that only pions are produced according to a statistical distribution. A system consisting of many pions produced in a single event may be decomposed into three subsystems, which consist of like sign pions, that is, π^+ , π^- and π^0 subsystems. For example, consider a π^+ subsystem in the longitudinal phase space with limited transverse momentum[10]. The longitudinal axis may be identified with the direction of the initial quark and antiquark produced by the virtual photon in center of mass system. Then the rapidity space in the longitudinal phase space is divided into many cells [11] of equal size δy , and we consider a probability to find π^+ mesons in each cell. The probability of finding n_i π^+ s in the i -th cell, $P_i^{(n_i)}$ is normalized as

$$\sum_{n_i=0}^{\infty} P_i^{(n_i)} = 1. \quad (1)$$

The summation index n_i runs from 0 to infinity because of the Bose-Einstein statistics. The mean π^+ multiplicity and the mean energy of the π^+ subsystem are given, respectively, by:

$$\langle n_+ \rangle = \sum_i \sum_{n_i} n_i P_i^{(n_i)} \quad (2)$$

and

$$\langle E_+ \rangle = \sum_i \sum_{n_i} n_i \epsilon_i P_i^{(n_i)}. \quad (3)$$

Here ϵ_i is the energy of a π^+ in the i -th cell:

$$\epsilon_i = m_T \cosh y_i, \quad (4)$$

$$y_i = y_{min} + (i - \frac{1}{2})\delta y, \quad (5)$$

$$y_{min} = -\ln \left[\frac{\sqrt{s} + \sqrt{s - 4m_T^2}}{2m_T} \right], \quad (6)$$

where y_i is the central rapidity value of the i -th cell, y_{min} is the kinematical minimum value of rapidity, $m_T = \sqrt{\langle p_T \rangle^2 + m_\pi^2}$ is the mean transverse mass, and \sqrt{s} is the total center of mass energy. The same argument applies to both π^- and π^0 subsystems. Therefore the mean multiplicities and the mean energies of those subsystems are given as

$$\langle n_+ \rangle = \langle n_0 \rangle = \langle n_- \rangle = \langle n_{ch} \rangle / 2, \quad (7)$$

and

$$\langle E_+ \rangle = \langle E_0 \rangle = \langle E_- \rangle = \sqrt{s}/3, \quad (8)$$

where $\langle n_{ch} \rangle$ is the mean charged multiplicity. The most probable distribution $P_i^{(n_i)}$ for the π^+ subsystem can be determined by the maximum entropy method which is well-known in information theory[8]. According to a statistical picture, particles will distribute in the phase space in such a way that every possible state is realized with the same probability. This method has been applied in many fields in science including multiparticle production phenomenology. First, we define the missing information entropy [9]:

$$S = - \sum_i \sum_{n_i} P_i^{(n_i)} \ln P_i^{(n_i)}. \quad (9)$$

This S has the maximum value when $P_i^{(n_i)}$ is a constant, so-called equal *a priori* probabilities, which does not depend on i and n_i . It is noted here that the probability $P_i^{(n_i)}$ does not depend on $P_j^{(n_j)}$ when $(i \neq j)$. Therefore a probability of finding n_i π^+ s in the i -th cell and n_j π^+ s in the j -th cell simultaneously, $P_{i,j}^{(n_i, n_j)}$, is given by

$$P_{i,j}^{(n_i, n_j)} = P_i^{(n_i)} \times P_j^{(n_j)}. \quad (10)$$

The entropy S should be maximized with the constraints which correspond to the normalization eq.(1), the mean multiplicity eq.(2) and the mean energy eq.(3) of the subsystems. For that purpose we consider F defined below instead of S by introducing Lagrange multipliers λ_1^i , λ_2 and λ_3 ;

$$\begin{aligned} F = & - \sum_i \sum_{n_i} P_i^{(n_i)} \ln P_i^{(n_i)} \\ & + \sum_i \lambda_1^i (\sum_{n_i} P_i^{(n_i)} - 1) \\ & + \lambda_2 (\sum_i \sum_{n_i} n_i P_i^{(n_i)} - \langle n_+ \rangle) \\ & + \lambda_3 (\sum_i \sum_{n_i} n_i \epsilon_i P_i^{(n_i)} - \langle E_+ \rangle) . \end{aligned} \quad (11)$$

By requiring that the variation of F is vanishing, one obtains

$$P_i^{(n_i)} = \frac{e^{n_i(\mu - \epsilon_i)/T}}{Z_i} . \quad (12)$$

Here, the Lagrange multipliers λ_1^i , λ_2 and λ_3 are rewritten in terms of the partition function Z_i , the “partition” temperature T [12] and the “chemical” potential μ :

$$e^{-1+\lambda_1^i} = 1 - e^{(\mu - \epsilon_i)/T} \equiv 1/Z_i , \quad (13)$$

$$\lambda_2 = \mu/T , \quad (14)$$

$$\lambda_3 = -1/T. \quad (15)$$

The parameters T and μ are determined uniquely for given $\langle E_+ \rangle$ and $\langle n_+ \rangle$ and they play a dominant role to reproduce the gross features of data on single particle spectra. The probability distribution functions for π^- and π^0 subsystems are the same as $P_i^{(n_i)}$ for π^+ subsystem. The parameter δy is determined by fitting to data on the second order fluctuations of multiplicity.

In order to study the resonance effect, we also consider another extreme case called ρ -model where it is assumed that only ρ mesons are produced in the same way as pions in the π -model. In the ρ -model, one must take the spin degree of freedom into account. A ρ meson system is decomposed into nine subsystems: $\rho^+\uparrow$, $\rho^+\rightarrow$, $\rho^+\downarrow$, $\rho^0\uparrow$, $\rho^0\rightarrow$, $\rho^0\downarrow$, $\rho^-\uparrow$, $\rho^-\rightarrow$, and $\rho^-\downarrow$, where \uparrow , \rightarrow , and \downarrow denote the three eigenstates of the spin $S_z = +1, 0$ and -1 , respectively. The partition temperature T_ρ , the “chemical potential” μ_ρ and the cell size δy_ρ in the ρ -model are determined so as to reproduce the mean charged multiplicity, the total energy and the second order fluctuations of multiplicity. (The decay process of ρ meson will be discussed in Sec. III B)

3 Method of simulation

The method of generating events based on the π -model and the ρ -model is explained in this section.

3.1 π -model

Events generating procedures are divided into three steps. The first step is determination of the parameters μ and T . The second step is δy search with trial events. By using these determined parameters, the final simulations are executed in the third step.

Step 1: Determination of the parameters μ and T

To determine the values of T and μ , we solve the following simultaneous equations for μ and T with a fixed trial value of δy :

$$\begin{aligned} \langle n_{ch} \rangle / 2 &= \sum_i \sum_{n_i} n_i \frac{e^{n_i(\mu - \epsilon_i)/T}}{Z_i} \\ &= \sum_i \frac{e^{(\mu - \epsilon_i)/T}}{1 - e^{(\mu - \epsilon_i)/T}}, \end{aligned} \quad (16)$$

$$\begin{aligned}
\sqrt{s}/3 &= \sum_i \sum_{n_i} n_i \epsilon_i \frac{e^{n_i(\mu - \epsilon_i)/T}}{Z_i} \\
&= \sum_i \frac{\epsilon_i e^{(\mu - \epsilon_i)/T}}{1 - e^{(\mu - \epsilon_i)/T}},
\end{aligned} \tag{17}$$

where observed value is used for the mean charged multiplicity $\langle n_{ch} \rangle$. It should be noted here that μ and T are determined as functions of δy , i.e. $\mu = \mu(\delta y)$, $T = T(\delta y)$.

Step 2: Generation of trial events and determination of the parameter δy

1. In order to avoid a possible artifact due to a particular cell location, we now take the central value y_i of the i -th cell as $y_i = y_{min} + (i - \frac{1}{2} + r)\delta y$, where r is a homogeneous random number between 0 and 1.
2. The π^+ , π^0 and π^- subsystems are generated in all cells in the rapidity space according to the probability distribution $P_i^{(n_i)}$ with a trial δy , $\mu(\delta y)$ and $T(\delta y)$. When a pion is produced in a certain cell, its rapidity is assigned by using a random number so that pions distribute homogeneously in that cell. This smearing of pion rapidity causes slight changes of $\langle n_{ch} \rangle$ and \sqrt{s} in comparison with the result of the step 1. We readjust the values of μ and T to reproduce correctly the mean multiplicity and the “mean” energy of the system.
3. Charge conservation is demanded event by event. Events are discarded if the charge conservation is violated.
4. The transverse momenta are generated according to the following distribution:

$$\frac{d\sigma}{dp_T} \propto p_T e^{-2p_T/\langle p_T \rangle} . \tag{18}$$

Here $\langle p_T \rangle$ denotes the observed mean transverse momentum at each \sqrt{s} .

The azimuthal angle φ of the transverse momentum is distributed at random between 0 and 2π . The transverse momenta generated in this way are assigned to all pions independent of their rapidities. A four momentum of a pion is then given as

$$\begin{aligned}
p^\mu &= (\sqrt{m_\pi^2 + p_T^2} \cosh y, p_T \cos \varphi, \\
&\quad p_T \sin \varphi, \sqrt{m_\pi^2 + p_T^2} \sinh y).
\end{aligned} \tag{19}$$

5. Approximate energy-momentum conservation is also required. For energy conservation, we set an energy window with width $\pm \delta E$ around \sqrt{s} . For momentum conservation, we also set the longitudinal and the transverse momentum windows with widths $\pm \delta P_L$ and δP_T , respectively, around 0 total momentum. The total energy E_{tot} , the longitudinal component of the total momentum P_L and the transverse component P_T are evaluated in every event. An event is adopted only when it satisfies the inequalities

$$\sqrt{s} - \delta E \leq E_{tot} = \sum_{all \ \pi} \epsilon \leq \sqrt{s} + \delta E, \tag{20}$$

and

$$-\delta P_L \leq P_L = \sum_{all \ \pi} p_L \leq \delta P_L, \quad (21)$$

$$\vec{P}_T^2 = \left| \sum_{all \ \pi} \vec{p}_T \right|^2 \leq (\delta P_T)^2. \quad (22)$$

As an example, the distribution of E_{tot} and the applied energy window for $\sqrt{s}=34.5$ GeV are shown in Fig.1. One has to take the window size as small as possible to keep the quality of conservation law while one would like to take it as large as possible to save the computation time. Thus one has to determine an optimum value of window size. We decided to take $\delta E = 0.2\sqrt{s}$ and $\delta P_L = 0.2p_{max}$, where p_{max} is the maximum value of the c.m. momentum carried by a pion. By the way, we found that some physical quantities, e.g., the dispersion of the multiplicity distributions are rather sensitive to δE when δE is large. We have confirmed that this strong δE -dependence disappears when $\delta E = 0.2\sqrt{s}$, which implies that the physical observables are insensitive to δE if $\delta E \leq 0.2\sqrt{s}$. For p_T -conservation, we use a multiplicity dependent window size $\delta P_T = \sqrt{n_+ + n_0 + n_-} \langle p_T \rangle$.

6. The jet axis, thrust or sphericity, is determined event by event. New four components of a momentum vector of a pion are calculated by referring to this jet axis.
7. The value of the parameter δy is determined by fitting to appropriate experimental data which are sensitive to δy . We have used the rapidity interval dependence of $D_{ch}^2/\langle n_{ch} \rangle^2$ for the fitting. Here, $D_{ch} = \sqrt{\langle n_{ch}^2 \rangle - \langle n_{ch} \rangle^2}$.

Figure 1.

Step 3: Final event generation

A sufficiently large number of events are generated using the probability distribution $P_i^{(n_i)}$ with μ , T and δy determined in the preceding steps.

Final results of those parameters are shown in Table I and the results of the fitting are shown in Fig.2(a)-(c), where y_{cut} is the half size of the rapidity interval $[-y_{cut}, y_{cut}]$. Experimental data are taken from refs.[13, 14]. As shown in Table I, 0.6, 0.8 and 1.2 are chosen as the values of the δy at $\sqrt{s} = 14.0, 34.5$ and 91.2 GeV, respectively. In the determination of the best fit value δy , we have put a special weight on the data point for $y_{cut} = y_{max}$ in order to reproduce the multiplicity distribution for full phase space as precisely as possible. It should be noted that y_{cut} dependence of the $D_{ch}^2/\langle n_{ch} \rangle^2$, a kind of 2nd order fluctuations of the particle density in the rapidity space, is reproduced well.

Figure 2. (a)-(c)
Table I

3.2 ρ -model.

The parameter T_ρ , μ_ρ and δy_ρ in the ρ -model are determined in a way similar to the π -model. The results are given in Table II.

Table II

Now we discuss the decay of ρ mesons e.g. $\rho^+ \rightarrow \pi^+\pi^0$. Rapidities have to be assigned to each pion produced from one ρ meson of some rapidity y_ρ . In the rest frame of the ρ meson, the maximum and the minimum rapidities of the two pions produced by the ρ meson are given by $\pm y_d$ where

$$y_d = \frac{1}{2} \ln\left(\frac{E_d + p_d}{E_d - p_d}\right), \quad (23)$$

$$E_d = \sqrt{p_d^2 + m_\pi^2}, \quad p_d = \sqrt{M_\rho^2/4 - m_\pi^2},$$

and M_ρ and m_π are the masses of the ρ and π mesons. We use the following Breit-Wigner form $f(M_\rho)$ as the invariant mass distribution of ρ meson:

$$f(M_\rho) \propto \frac{1}{(M_\rho - m_\rho)^2 + \Gamma^2/4}, \quad (24)$$

where $m_\rho=770$ MeV and $\Gamma=150$ MeV.

To impose the Bose-Einstein correlations between like charge pions, we use an “enhancement factor” method. When a parent ρ meson has a rapidity y_ρ , we divide the longitudinal rapidity interval $[y_\rho - y_d, y_\rho + y_d]$ into K cells of equal size δy_π . Here we take $\delta y_\pi = \delta y$. In order to determine the cell to which a pion, say π^+ , belongs, we introduce the enhancement factor:

$$\frac{n_i^+ + 1}{K + N^+} \quad \text{for } i\text{-th cell}, \quad (25)$$

where n_i^+ and N^+ are the number of π^+ s already produced in the i -th cell and that in the interval $[y_\rho - y_d, y_\rho + y_d]$, respectively. Transverse momenta \vec{p}_{T1} and \vec{p}_{T2} are assigned to the two pions, in the same way as in the π - model. To reproduce the invariant mass of the parent ρ meson M_ρ , the azimuthal angle difference, $\Delta\phi = \phi_1 - \phi_2$, needs to satisfy the following equation:

$$M_\rho^2 = 2m_\pi^2 + 2(\epsilon_1\epsilon_2 - p_{L1}p_{L2} - |\vec{p}_{T1}||\vec{p}_{T2}| \cos \Delta\phi), \quad (26)$$

$$\epsilon_i = \sqrt{m_\pi^2 + |\vec{p}_{Ti}^2|} \cosh y_i, \quad (27)$$

$$p_{Li} = \sqrt{m_\pi^2 + |\vec{p}_{Ti}^2|} \sinh y_i \quad \text{for } i = 1 \text{ or } 2. \quad (28)$$

4 Comparison of results with experimental data

In this chapter we compare the results of event simulation with experimental data. We investigate effects of charge and energy-momentum conservations and also the resonance

effect by comparing the results from π - and ρ - models. 20000 events of multiparticle production in e^+e^- annihilation have been generated for both the π -model and the ρ -model at each energy $\sqrt{s} = 14.0, 34.5$ and 91.2 GeV. We use the experimental data reported by the TASSO Collaboration[13, 15, 16, 17] for $\sqrt{s} = 14.0, 34.5$ GeV, and by the DELPHI [14, 18, 19, 20] and ALEPH Collaborations[21, 22] for 91.2 GeV. We present all results obtained from the π -model. When significant differences are found between the two models, we present also the result of the ρ - model.

4.1 Multiplicity distributions

Charged multiplicity distributions $P(n_{ch})$ are shown in Figs.3 (a)-(c). The experimental data[13, 14] are well reproduced by our π -model. This is reasonable because the mean multiplicity and dispersion of the multiplicity distribution are used in the determination of the model parameters. It should be noted, however, that our model is able to predict the detailed shape of the multiplicity distribution at each energy. We also investigate the multiplicity distribution in terms of KNO variable. Our model gives good scaling behavior for both the full phase space(see Fig.4(a)) and small rapidity windows(not shown). The y_{cut} -dependence of the multiplicity distribution is reproduced correctly as shown in Fig.4(b). Note that our results are approximately consistent with the negative binomial distributions.

Figure 3. (a)-(c)
Figure 4. (a) and (b)

Dependence of multiplicity distributions on δy has already been demonstrated in Figs.2(a)-(c). Decreasing δy reduces the dispersion of the multiplicity distribution. Conservation laws also affect the multiplicity distribution. In addition to “full conservation” event for which both energy-momentum and charge conservation are imposed, we have also generated events with “only charge conservation”, “only energy-momentum conservation” or “no conservation” by imposing only charge conservation or only energy-momentum conservation or none of them in order to investigate the effects of conservation laws¹. It is found that the charge conservation causes the broadening of the multiplicity distribution, while the effect of energy conservation is opposite as shown in Fig.5. The effect of energy-momentum conservation is stronger than that of charge conservation.

We have investigated the charge correlations due to charge conservation. For this purpose, we consider the rapidity window dependence of the quantity $D_{ch}^2/2D_+^2$, where D_+^2 is the dispersion of the π^+ multiplicity distribution, $\sqrt{\langle n_+^2 \rangle - \langle n_+ \rangle^2}$. The quantity $D_{ch}^2/2D_+^2$ can be written as

$$\begin{aligned} \frac{D_{ch}^2}{2D_+^2} &= \frac{\langle (n_+ + n_-)^2 \rangle - \langle n_+ + n_- \rangle^2}{2D_+^2} \\ &= 1 + \frac{\langle n_+ n_- \rangle - \langle n_+ \rangle^2}{D_+^2}, \end{aligned}$$

¹ It should be noted here that both energy-momentum and charge conservations hold on the average even in events with no conservation.

where use was made of the equality $\langle n_+ \rangle = \langle n_- \rangle$. If there is the maximum correlation $n_+ = n_-$ due to charge conservation, one has $D_{ch}^2/2D_+^2 = 2$ because $\langle n_+ n_- \rangle = \langle n_+^2 \rangle$. On the other hand, if there is no correlation between n_+ and n_- , $\langle n_+ n_- \rangle$ is reduced to $\langle n_+ \rangle^2$ and hence $D_{ch}^2/2D_+^2 = 1$. Therefore, it is obvious that $D_{ch}^2/2D_+^2 = 2$ for $y_{cut} = y_{max}$. On the other hand, one can expect that $D_{ch}^2/2D_+^2 = 1$ for very small y_{cut} because the correlation due to charge conservation will be maximally weakened when y_{cut} is small. Those expectations are indeed realized by our simulation as shown in Fig.6. The correlation measure $D_{ch}^2/2D_+^2$ increases linearly from about unity as y_{cut} increases and then tends to saturate at the value 2 for $y_{cut} \geq 3.5$. The slope of the linear rise may be regarded as a measure of local charge conservation. Unfortunately, it appears that corresponding experimental data are not available at present. We therefore urge experimentalists to provide such data.

Figure 5
Figure 6 (a) and (b)

4.2 Rapidity distribution

The single particle rapidity distributions are calculated and the results are shown in Fig.7. Our model reproduces the experimental data[15] except for the observed dip structure at $y \cong 0^2$. In particular, the energy dependence of the central height is reproduced correctly by our model. Although our model produces a dip at $y=0$ in qualitative agreement with experimental data, it is too deep and too narrow. Furthermore it tends to diminish as \sqrt{s} increases. This tendency appears opposite to what is observed experimentally. This situation does not change even if one uses the ρ - model. The discrepancy may be due to the fact that three jet events are not included in our model³. By the way, we found that the dip is not reproduced if one uses the sphericity instead of the thrust to define the jet axis. We have also confirmed that the rapidity distribution is insensitive to both conservation laws and the value of δy .

Figure 7.

4.3 Rapidity dependence of the mean transverse momentum

There are interesting experimental data on the rapidity dependence of the mean transverse momentum, $\langle p_T(y) \rangle$ [15]. The observed $\langle p_T(y) \rangle$ is almost constant in the central region while it decreases as y approaches the kinematical limit as shown in Fig.8(a). On the other hand, transverse momentum of a pion is generated according to the exponential formula (18) with y -independent mean transverse momentum $\langle p_T \rangle$ in our model. Therefore, it is very interesting to see if our model can reproduce the observed y -dependence of the

² The result of our model is systematically larger than TASSO data at $\sqrt{s}=14.0$ and 34.5 GeV, because integration of the dn/dy data reported by TASSO is smaller than the reported mean multiplicity.

³ This dip structure had been investigated by TASSO collaboration[15]. They report their analyses using the Lund-string model[23] and the independent jet model[24].

mean transverse momentum. The result of our model is shown and compared with data in Fig.8(a). Our model reproduces correctly the observed y -dependence of the mean transverse momentum. Therefore, one can conclude that the observed y -dependence is totally due to kinematical reasons. To confirm this conclusion, we have calculated $\langle p_T(y) \rangle$ for events generated without energy-momentum conservation and/or without assigning the thrust axis. The result for 34.5 GeV is shown in Fig. 8(b). It is clearly seen that the energy-momentum conservation is most responsible for reproducing the correct y -dependence but the use of thrust axis has also some effect.

Figure 8. (a) and (b)

4.4 Bin size dependence of the scaled factorial moments

We study the scaled factorial moments in order to investigate the fluctuations of particle density in the rapidity space. The following two kinds of scaled factorial moment are used for comparison with experimental data.

The factorial moments are evaluated for the multiplicity of particles produced in the rapidity window $y_0 \leq y \leq y_0 + \Delta Y$. The rapidity window is divided into M bins of equal size $\Delta Y/M$. When N particles are produced in the window while k_m particles are found in the m -th bin, the ‘exclusive’ scaled factorial moment[2] is defined as

$$F_i^{ex} = M^{i-1} \left\langle \sum_{m=1}^M \frac{k_m(k_m-1) \cdots (k_m-i+1)}{N(N-1) \cdots (N-i+1)} \right\rangle, \quad (29)$$

where $\langle \rangle$ means an event average with fixed N . The ‘inclusive’ scaled factorial moment used in many literatures[3] is given by

$$F_i^{in} = M^{i-1} \left\langle \sum_{m=1}^M \frac{k_m(k_m-1) \cdots (k_m-i+1)}{\langle N \rangle^i} \right\rangle, \quad (30)$$

where $\langle \rangle$ now means an event average for distributed N . Both F_i^{ex} and F_i^{in} are equal to unity if there are only statistical fluctuations(a binomial distribution for F_i^{ex} or a Poisson distribution for F_i^{in}). On the other hand, the Bose-Einstein distribution (eq.(12)) gives a typical example of non-statistical fluctuations. It is the multiplicity distribution in a single cell of size δy in our model, corresponding to $M \approx \Delta Y/\delta y$. In this case the inclusive factorial moments of the second order for like charged and all charged particles are given, respectively, by

$$\begin{aligned} F_2^{in} &= \frac{\langle n_+(n_+ - 1) \rangle}{\langle n_+ \rangle^2} \\ &= 2 \quad (\text{for like sign particles}) , \end{aligned} \quad (31)$$

and

$$\begin{aligned} F_2^{in} &= \frac{\langle (n_+ + n_-)^2 - (n_+ + n_-) \rangle}{\langle (n_+ + n_-) \rangle^2} \\ &= \frac{\langle n_+(n_+ - 1) \rangle + \langle n_+ \rangle^2}{2\langle n_+ \rangle^2} \\ &= 1.5 \quad (\text{for charged particles}) . \end{aligned} \quad (32)$$

For $\sqrt{s}=34.5\text{GeV}$, one can investigate the fluctuations in a single cell, i.e. fluctuations induced by pure Bose-Einstein distributions(cf. eq (32)) at $M=5$ since $\delta y=0.8$ and $\Delta Y=4.0$. Our simulation gives $F_2^{in}(M=5) \approx 1.27$, and $F_2^{in}(M>16) \approx 1.38$. The reduction from 1.5 can be attributed to the smearing due to varying cell location(cf. the item 1 of the step 2 of sec.III A) and also to the global charge conservation. In fact, we obtain $F_2^{in}(M=5) \approx 1.32$, and $F_2^{in}(M>16) \approx 1.46$ when all the conservation laws are not imposed.

Now the results are compared with experimental data[16, 21] for both exclusive and inclusive factorial moments in Figs. 9 and 10. Our results approximately reproduce the experimental data. In particular, the agreement is very good for $\sqrt{s} = 34.5$ GeV. In our model, the parameter δy plays a crucial role in reproducing the bin size dependence of the factorial moments. As M increases from unity, the factorial moments increase due to the BEC and then start to saturate for $M > \Delta Y/\delta y^4$. In this sense, the parameter δy in our model may be interpreted as an effective correlation length in the rapidity space due to the BEC. Our results show that the BEC considerably contribute to the increase of the scaled factorial moments(the so-called intermittency). However, at $\sqrt{s} = 91.2$ GeV our results of both exclusive and inclusive factorial moment systematically underestimate compared with experimental data for all orders. This underestimation becomes remarkable as the order of the moment increases. It may be due to three jets events at high energy not taken into account in our calculation. At LEP energy, events with three jets take place with a significant probability.

Figure 9. (a)-(c)
Figure 10. (a)-(c)

4.5 Bose-Einstein correlations

Here the results for the Bose-Einstein correlation functions are compared with data at $\sqrt{s} = 34.5$ [17], and 91.2 GeV [19, 22]. The following correlation functions $C(Q)$ (or $C(Q^2)$) are used for this analysis:

$$C(Q) = N^{\pm\pm}(Q)/N^{ref}(Q) \quad \text{or} \quad C(Q^2) = N^{\pm\pm}(Q^2)/N^{ref}(Q^2), \quad (33)$$

where $N^{\pm\pm}(Q)$ (or $N^{\pm\pm}(Q^2)$) is the number of like sign pairs with four momentum difference: $Q^2 = (p_1 - p_2)^2$ or $Q = \sqrt{Q^2}$. The so-called reference sample, the denominator N^{ref} is the number of pairs without Bose-Einstein correlations. TASSO and ALEPH collaboration use the number of unlike sign pairs as N^{ref} . ‘Mixed pair reference’ is also used by ALEPH. In this case, a pair is taken from different events. Our results of both the π - and the ρ - models are shown in Figs. 11 and 12, respectively. We also present energy dependence of the BEC correlation function $C(Q)$ in Figs.13(a) for the π -model and (b) for the ρ -model.

⁴ TASSO Collaboration compared their data[16] (exclusive factorial moments at $\sqrt{s} = 34.5$ GeV) with results of various event simulators of multiparticle production model: Webber, Hoyer and Lund model version 6.2 and 6.3 (see Refs in [16]). Those models can also roughly reproduce the experimental data. The BEC are not taken into account while cascade processes are included in them.

Figure 11. (a),(b)
Figure 12.

Our model produces a characteristic enhancement of $C(Q)$ ($C(Q^2)$) in small Q (Q^2) region. The result of the ρ -model is in better agreement with experimental data than the π -model for the whole region of Q^2 . We found that the enhancement of the correlation function $C(Q)$ ($C(Q^2)$) strongly depends on the size of δy . When δy becomes large, the slope of the correlation function becomes small. If δy is larger than the rapidity interval for the full phase space, i.e. $\delta y \geq 2y_{\max}$, the correlation function has no Q dependence, $C(Q) \equiv 2$. On the contrary when δy approaches to zero, the slope of the correlation function becomes large and $C(Q)$ approaches to unity for $Q > 0$.

Although our model has no explicit information on the space-time structure of particle emission points, we can extract the size and the lifetime of the particle sources by fitting a theoretical formula to the result with mixed pair reference from our simulation. Here we use the following fitting formula for $Q > 5$ MeV/c:

$$C(Q) = c[1 + \lambda \exp(-RQ)], \quad (34)$$

$$C(Q^2) = c[1 + \lambda \exp(-R^2 Q^2)], \quad (35)$$

where c is the normalization constant, λ is the so-called chaoticity parameter, and R is the size parameter. We don't use data for $Q < 5$ MeV/c in the fitting because the statistical errors are very large there.

Figure 13. (a) and (b).

In Table III, the results of the fitting at various energies are summarized for both the π -model and the ρ -model. With increasing energy of the system, R decreases while λ tends to increase. We find that R in the ρ -model is larger than that in the π -model. We also try to extract the longitudinal size R_L , transverse size R_T , and lifetime τ by using the following formulae in our fit:

$$\begin{aligned} C(Q_L) &= c_L[1 + \lambda_L \exp(-R_L^2 Q_L^2)], & C(Q_T) &= c_T[1 + \lambda_T \exp(-R_T^2 Q_T^2)], \\ C(\Delta E) &= c_\tau[1 + \lambda_\tau \exp(-\tau^2 \Delta E^2)], \end{aligned} \quad (36)$$

where $Q_L^2 = |p_{L1} - p_{L2}|^2$, $Q_T^2 = |\vec{p}_{T1} - \vec{p}_{T2}|^2$ and $\Delta E = |\epsilon_1 - \epsilon_2|$. The results are presented in Table IV. The source size decreases with increasing \sqrt{s} , while the life time is almost independent of \sqrt{s} . It is reasonable that $C(Q_T)$ has no strong Q_T -dependence because the BEC is not taken into account in the transverse momentum space in our model.

Table III and IV

The value of the normalization constant c may be understood as follows. The number of unlike charged pairs and that of $(++)$ pairs for large Q may be proportional to

(statistical) combinatorial numbers $\langle n_+ n_- \rangle$ and $\langle n_+ (n_+ - 1) \rangle$, respectively. Therefore the asymptotic value of the correlation function may be estimated as

$$\lim_{Q \rightarrow \infty} C(Q) \equiv c \quad (37)$$

$$\begin{aligned} &\cong \frac{\langle n_+ (n_+ - 1) \rangle}{\langle n_+ n_- \rangle} \\ &\cong 1 - \frac{\langle n_+ \rangle}{\langle n_+^2 \rangle} \end{aligned} \quad (38)$$

where we have used charge conservation in deriving the second line. Eq. (38) with the approximation $\langle n_+^2 \rangle \sim \langle n_+ \rangle^2$ and the experimental values of $\langle n_{ch} \rangle (= 2\langle n_+ \rangle)$ yields $c=0.785$, 0.855 and 0.901 for $\sqrt{s}=14.0$, 34.5 and 91.2 GeV, respectively in qualitative agreement with the result given in Table III.

We also investigate the influence of the charge and energy-momentum conservation on the Bose-Einstein correlations. Both energy-momentum conservation and charge conservation reduce the values of the correlation functions in the whole Q (or Q^2) range as shown in Fig.14. The effect of charge conservation is stronger than that of energy-momentum conservation. If “no conservation” events are used, $C(Q)$ approaches to a larger constant as Q increases.

Figure 14.

As mentioned in Section III B, the BEC in the ρ -model is imposed for like-charged pions by using the enhancement factor. By changing this enhancement factor, we can control the strength of the BEC. For example, one can reduce the BEC substantially by putting $n_i^+ = N^+ = 0$ in eq.(25) as shown in Fig.15.

Figure 15.

4.6 2-particle rapidity correlations

We investigate the 2-particle correlations in terms of rapidity variables in detail. The experimental data reported by TASSO Collaboration[17] at $\sqrt{s}=34.5$ GeV is used in comparison with our calculations. When the 2-particles of type “ a ” and “ b ” (for example, $a, b = \pi^+, \pi^-$) have rapidities y_1 and y_2 , respectively, the two particle rapidity correlation function $R_2^{(a,b)}(y_1, y_2)$ is defined as follows:

$$R_2^{(a,b)}(y_1, y_2) \equiv \frac{\rho^{(a,b)}(y_1, y_2)}{f \rho^{(a)}(y_1) \rho^{(b)}(y_2)} - 1, \quad (39)$$

where $\rho^{(a,b)}(y_1, y_2)$ and $\rho^{(a)}(y_1)$ is the two particle density and the one particle density, respectively:

$$\rho^{(a,b)}(y_1, y_2) = \frac{1}{\sigma} \frac{d^2 \sigma}{dy_1 dy_2}, \quad (40)$$

$$\rho^{(a)}(y_1) = \frac{1}{\sigma} \frac{d\sigma}{dy}. \quad (41)$$

Here σ is the total cross section and f is the normalization constant given by

$$f = \frac{\langle n_a(n_b - \delta_{ab}) \rangle}{\langle n_a \rangle \langle n_b \rangle}, \quad (42)$$

where

$$\delta_{ab} = \begin{cases} 1 & \text{for } a=b \\ 0 & \text{for } a \neq b \\ 0 & \text{when particle type is not distinguished,} \end{cases} \quad (43)$$

and n_a and n_b are the multiplicities of “ a ” and “ b ”, respectively.

Instead of using $R_2^{(a,b)}(y_1, y_2)$, in practical measurements by TASSO Collaboration, they use

$$R_2^{(a,b)}(y_1, y_{trigg}) \equiv \frac{1}{y_\beta - y_\alpha} \int_{y_\alpha}^{y_\beta} dy_t R_2^{(a,b)}(y_1, y_t), \quad (44)$$

where y_{trigg} refers to a rapidity interval (y_α, y_β) . These trigger rapidity intervals are trigger I ($-5.50 \leq y \leq -2.50$), trigger II ($-2.50 \leq y \leq -1.50$), trigger III ($-1.50 \leq y \leq -0.75$) and trigger IV ($-0.75 \leq y \leq -0.00$). First we investigate a case where sign of charge is not distinguished and hence $\delta_{ab}=0$. The results are compared with experimental data in Fig.16(a)-(d). The experimental data are approximately reproduced by the simulation for every trigger regions. Although our model predicts a negative correlation for large y ($y \geq 2$) in the trigger I, a positive correlation is reported by TASSO. For the trigger regions II, III and IV, calculated correlation functions show positive bumps around the trigger rapidity interval in agreement with experiment. The effect is apparently caused by the BEC.

Figure 16(a)-(d)

For confirmation, we calculate the 2-particle rapidity correlation $R^{++}(y, y_{trigg})$ and $R^{+-}(y, y_{trigg})$. See Fig.17(a)-(d). The clear positive correlations are seen near the trigger rapidities in the correlation function $R^{(++)}(y_1, y_2)$. On the other hand, such positive correlations are absent in $R^{(+-)}(y_1, y_2)$. From these investigations, one can conclude that the BEC (identical particle effect) plays a crucial role in an enhancement of the $R^{++}(y, y_{trigg})$ near the trigger rapidity y_{trigg} . The correlation functions are also affected by the effects of ρ meson production and their decay. Results of the ρ -model are shown in Fig.18. It is found that the ρ -model gives better agreement with experimental data than the π -model for all trigger rapidity intervals.

Figure 17 (a)-(d)

There are some discrepancies between the model result for $R(y, y_{trigg})$ and the data as most evidently seen in Fig.16(a). The situation is qualitatively the same in both the π - and the ρ - models. This is an indication that there are unknown long range as well as short range correlations besides BEC, e.g. those due to higher resonances and/or three jets.

Figure 18. (a)-(d)

In analogy to $C(Q)$, another 2-particle rapidity correlation function can be defined by using the rapidity difference $\Delta y = |y_1 - y_2|$ in place of Q :

$$\tilde{C}(\Delta y) \equiv \frac{N^{++}(\Delta y)}{N^{ref}(\Delta y)}. \quad (45)$$

This function allows us to measure the size of the model parameter δy . We expect that slope of $\tilde{C}(\Delta y)$ will change at $\Delta y \approx \delta y$. In this paper, we assume that δy is independent of y . This assumption can be checked by measuring $\tilde{C}(\Delta y)$ in various rapidity regions. We strongly urge experimentalists to measure $\tilde{C}(\Delta y)$. Our prediction for this correlation function is shown in Fig.19(a)-(c).

Figure 19.

4.7 Forward-backward correlations

Finally we compare the results of the forward-backward correlation with experimental data[13, 20]. It is known experimentally that there are weak (positive) correlations between the multiplicity n_B in the backward hemisphere and the mean multiplicity $\langle n_F \rangle$ in the forward hemisphere. The direction of the “forward” or “backward” is assigned at random in the simulation. The comparison of our results with experimental data is shown in Fig.20. It is found that our model reproduces well experimental data for every \sqrt{s} . This correlation is usually parameterized by a linear form:

$$\langle n_F \rangle = a + b n_B. \quad (46)$$

The values of the parameters a and b extracted from the π -model and the corresponding experimental values are given in Table V.

Figure 20.
Table V

The correlation strength b depends on the size of δy . When δy becomes large, the correlation strength b also becomes large. When the multiplicity distribution is extremely narrow, the correlation strength b is negative. For example, if the multiplicity distribution is delta function type, $P(n_{ch}) = \delta(n_{ch} - \langle n_{ch} \rangle)$, the correlation strength b is -1 . Note that the dispersion of the multiplicity distribution is also sensitive to the size of δy . Increase of δy enhances the dispersion of the multiplicity distribution. This enhancement of the dispersion also increases the correlation strength b . We found that the forward-backward correlation is not significantly affected by the energy-momentum conservation.

5 Conclusions and discussions

We have investigated various correlations and fluctuations observed in multiparticle production in e^+e^- annihilation by using a new statistical model constructed on the basis of the maximum entropy method. This model allows us to investigate the crucial roles of the Bose-Einstein Correlations (BEC) in multiparticle production phenomena. The model has three parameters T , μ and δy . The “partition” temperature T and the “chemical” potential μ characterize the single particle spectra. The BEC is characterized by the third parameter δy . Based on this model we have constructed two kinds of event generators which correspond to two extreme cases. One case is the π -model which assumes that all pions are produced directly, i.e., $e^+e^- \rightarrow \pi \pi \cdots$. The other is the ρ -model where it is assumed that all pions are produced via the decay of ρ mesons, i.e., $e^+e^- \rightarrow \rho \rho \cdots \rightarrow \pi \pi \cdots$. In the course of the event generation, energy-momentum and charge conservations are imposed by event selection. Thus we can study the effects on single particle spectra and correlations caused by these conservation laws. We found that some observables are significantly affected by them.

Various kinds of the experimental data on single particle spectra and many particle correlations are well reproduced by our model. We have compared the results obtained from our simulations with experimental data on multiplicity distributions, rapidity distributions and rapidity dependence of the mean transverse momentum. For many particle correlations, we compare our calculations with experimental data on factorial moments, Bose-Einstein correlations, 2-particle rapidity correlations and forward-backward correlations. We have also calculated the charge correlations in the rapidity space. We hope experimentalists will measure this observable.

Our results for all observables on correlations, including the dispersion of the multiplicity distributions, exhibit a strong δy dependence. We found that δy plays an essential role in explaining the behavior of some 2-particle correlation functions, scaled factorial moments and so on. Once the value of the parameter δy is determined by fitting our result on the rapidity dependence of the dispersion of the multiplicity distribution to that of the experimental data, other correlation and fluctuation data are systematically reproduced by using the same δy value. The parameter δy may correspond to an effective correlation length (in the rapidity space) of the BEC. Constancy of the size of the δy in the whole rapidity space is the most characteristic point in our model. This simple assumption may be checked by measuring the correlation $\tilde{C}(\Delta y)$ at various rapidity regions. There are possibilities that it depends on the rapidity y and/or the multiplicity.

In Bose-Einstein correlations and 2-particle rapidity correlations, in particular, we observe a clear difference between the prediction from the π -model and that from the ρ -model. We found that the ρ -model gives better agreement with those experimental data than the π -model. This means that two-particle correlations are sensitive to production and decay processes of resonances and experimental data on those observables suggest that there are significant contribution from resonance decay. No significant difference between the π -model and the ρ -model is observed in the single particle spectra and other correlation data.

Finally, we would like to point out two important aspects of our model. First, we

would like to emphasize that the BEC are incorporated on event-by-event basis in our model. It thus provides a useful theoretical tool for event-by-event analysis of the BEC. This is an important feature of our model not shared by any other event generators. Second, information on the space-time structure of multiparticle production is apparently not contained in our statistical model. Nevertheless, it gives the BEC from which one can extract the information on the “apparent” source size and the chaoticity. It thus appears that the information on the space-time structure is “hidden” in our model. The fundamental parameter δy may have some relevance to the question.

References

- [1] See for example,
D. H. Boal, Rev.Mod.Phys,**62**(1990), 553; M. Gyulassy, S. K. Kauffmann and L. W. Wilson, Phys.Rev.**C20**(1979), 2267; B. Lörstad, Int.J.Mod.Phys.**A4**(1989), 2861.
- [2] A. Bialas and P. Peschanski, Nucl.Phys.**B273**(1986), 703.
- [3] A. Bialas and P. Peschanski, Nucl.Phys.**B308**(1988), 857.
- [4] M. G. Bowler, Z.Phys. **C29** (1986), 617.
- [5] S. Pratt, Phys.Rev.Lett.**53**,(1984), 1219; J. P. Sullivan, Phys.Rev.Lett.**70**,(1993), 3000.
- [6] B. Andersson and W. Hofmann, Phys.Lett.**169B**(1986), 364; M. G. Bowler, Phys.Lett.**180B**(1986), 299; X. Artru and M. G. Bowler, Z.Phys.**C37**(1988), 293.
- [7] K. Kadija, P. Seyboth, Phys.Lett.**B287**(1992), 363; S. Haywood, RAL-94-07, July 1994.
- [8] E. T. Jaynes, Phys.Rev.**106**(1957), 620.
- [9] F. Takagi and T. Tsukamoto, Phys.Rev.**D38**(1988), 288; G. Wilk and Z. Włodarczyk Phys.Rev.**D43**(1991), 794.
- [10] See for example, L. Van Hove, Rev.Mod.Phys.**36**(1964), 655; Nucl.Phys.**B9**(1969), 331; A. G. Frodesen and P. Nybrog, Nucl.Phys.**B81**(1974), 283.
- [11] W. J. Knox, Phys.Rev.**D10**,(1974), 65; A. Giovannini, Nouvo Cim.**A15**(1973), 543; P. Carruthers and C.C.Shih, Phys.Lett.**B127**(1983), 242; A. Giovannini, L. Van Hove, Z.Phys.**C30**(1986), 391.
- [12] T. T. Chou, C. N. Yang and E.Yen, Phys.Rev.Lett **54**(1985), 510; T. T. Chou and C. N. Yang, Phys.Rev.**D32**(1985), 1692.
- [13] TASSO Collab., W. Braunschweig et al, Z.Phys.**C45**(1989), 193.
- [14] DELPHI Collab., P. Abreu et al, Z.Phys.**C52**(1991), 271.
- [15] TASSO Collab., M. Althoff et al, Z.Phys.**C22**(1984), 307.

- [16] TASSO Collab., W. Braunschweig et al, Phys.lett.**B231**(1989), 548.
- [17] TASSO Collab., M. Althoff et al, Z.Phys.**C29**(1985), 347.
- [18] DELPHI Collab., P. Abreu, et al, Phys.Lett. **247**(1990), 137.
- [19] DELPHI Collab., P. Abreu et al, Phys.Lett.**B286** (1992), 201.
- [20] DELPHI Collab., P. Abreu et al, Z.Phys.**C50**(1991), 185.
- [21] ALEPH Collab., D. Decamp, et al, Z.Phys.**C53** (1992), 21.
- [22] ALEPH Collab., D. Decamp et al, Z.Phys.**C54**(1992), 75.
- [23] B. Andersson, G. Gustafson, T.Sjöstrand, Phys.Lett.**B94**(1980), 211.
- [24] P. Hoyer et al, Nucl.Phys.**B161**(1979), 34; A. Ali et al, Z.Phys.**C2**(1979), 33.

Table captions

Table I: Best fit values of μ , T and δy for various \sqrt{s} with the observed values of $\langle n_{ch} \rangle$ and $\langle p_T \rangle$ used in the π -model.

Table II: Values of the parameters in the ρ -model.

Table III: The results of R , λ and c in the π - and the ρ - models.

Table IV: The results of R_L , R_T and τ in the π -model. Corresponding results of the chaoticity parameters λ_L , λ_T and λ_τ are also presented.

Table V: The results of the parameters which characterize the forward-backward correlation. The experimental values are given in the parentheses.

Figure captions

Fig.1: Total energy of events generated for the mean total energy $\langle E_{tot} \rangle = \sqrt{s} = 34.5$ GeV and the energy window of the full width $2\delta E = 0.4\sqrt{s}$.

Fig.2: Comparison of the results of the π -model with the experimental data on the y_{cut} dependence of $D_{ch}^2/\langle n_{ch} \rangle$ for (a) $\sqrt{s}=14.0$ GeV, (b) 34.5 GeV and (c) 91.2 GeV.

Fig.3: Comparison of multiplicity distributions in the π -model for (a) $\sqrt{s}=14.0$ GeV, (b) 34.5 GeV and (c) 91.2 GeV.

Fig.4 (a): KNO scaling of the multiplicity distributions in the π - model at energies $\sqrt{s}=14.0$, 34.5 and 91.2 GeV. (b): Comparison of the π - model (solid line) with the experimental data for energy $\sqrt{s}=91.2$ GeV with $y_{cut} \sim 6.5$ (full phase space), 2.0 and 1.0.

- Fig.5:** Effects of conservation laws on y_{cut} dependence of $D_{ch}^2/\langle n_{ch} \rangle^2$.
- Fig.6** (a): Prediction of charge correlation $D_{ch}^2/2D_+^2$ for $\sqrt{s} = 14.0, 34.5$ and 91.2 GeV. (b): Effects of conservation laws on charge correlation $D_{ch}^2/2D_+^2$.
- Fig.7:** Rapidity distribution dN/dy for $\sqrt{s} = 14.0, 34.5$ and 91.2 GeV in the π -model(open squares). Experimental data for $\sqrt{s} = 14.0$ and 34.5 GeV are shown by solid circles.
- Fig.8** (a): Rapidity dependence of the mean transverse momentum $\langle p_T \rangle$ for $\sqrt{s} = 14.0, 34.5$ and 91.2 GeV. (b): Effect of the thrust axis and/or the energy-momentum conservation for energy $\sqrt{s} = 34.5$ GeV.
- Fig.9:** The exclusive factorial moment for (a) $\sqrt{s} = 14.0$, (b) 34.5 GeV and (c) 91.2 GeV in the π -model(solid line). Experimental data are shown by open circles.
- Fig.10:** The same as in Fig.9(a)-(c) for the inclusive factorial moments in the π -model.
- Fig.11:** Comparisons of the results for $C(Q^2)$ from the π - and ρ - model with the experimental data for (a) $\sqrt{s} = 34.5$ GeV and (b) $\sqrt{s} = 91.2$ GeV. The number of unlike pairs is used as the reference.
- Fig.12:** The same as in Fig.11 for $\sqrt{s} = 91.2$ GeV with the mixed pairs as the reference sample.
- Fig.13:** Energy dependence of $C(Q)$ with mixed pair reference in the (a) π - and (b) ρ -models.
- Fig.14:** Effect of conservation laws on the BEC correlation function $C(Q)$.
- Fig.15:** The role of the enhancement factor in the ρ - model.
- Fig.16** (a): Comparison of the result from the π -model with experimental data on the 2-particle rapidity correlation function $R(y, y_{trigg})$ at $\sqrt{s} = 34.5$ GeV for (a) the trigger I $[-5.50, -2.50]$, (b) the trigger II $[-2.50, -1.50]$, (c) the trigger III $[-1.50, -0.75]$ and (d) the trigger IV $[-0.75, 0.00]$.
- Fig.17:** The 2-particle rapidity correlation functions $R^{++}(y, y_{trigg})$ and $R^{+-}(y, y_{trigg})$ in the π -model for $\sqrt{s} = 34.5$ GeV with (a) the trigger I $[-5.50, -2.50]$, (b) the trigger II $[-2.50, -1.50]$, (c) the trigger III $[-1.50, -0.75]$ and (d) the trigger IV $[-0.75, 0.00]$.
- Fig.18:** Comparison of the results of ρ - model with experimental data on the 2-particle rapidity correlation function $R(y, y_{trigg})$ at $\sqrt{s} = 34.5$ GeV for (a) the trigger I $[-5.50, -2.50]$, (b) the trigger II $[-2.50, -1.50]$, (c) the trigger III $[-1.50, -0.75]$ and (d) the trigger IV $[-0.75, 0.00]$.
- Fig.19:** Predictions for the 2-particle rapidity correlation function $\tilde{C}(\Delta y)$ for $\sqrt{s} = 14.0, 34.5$ and 91.2 GeV.
- Fig.20:** Comparison of the forward-backward correlation in the π -model with experimental data for $\sqrt{s} = 14.0, 34.5$ and 91.2 GeV.

\sqrt{s} [GeV]	δy	μ [GeV]	T [GeV]	$\langle n_{ch} \rangle$	$\langle p_T \rangle$ [GeV]
14.0	0.60	-1.71	2.47	9.30	0.334
22.0	0.70	-2.43	4.26	11.30	0.377
34.5	0.80	-3.08	5.75	13.59	0.422
43.6	0.85	-3.77	7.83	15.08	0.446
91.2	1.20	-4.73	15.4	20.80	0.521

Table I

\sqrt{s} [GeV]	δy_ρ	δy_π	μ_ρ [GeV]	T_ρ [GeV]
14.0	1.20	0.60	-3.61	3.05
34.5	1.60	0.80	-10.64	9.00
91.2	2.40	1.20	-17.34	20.27

Table II

\sqrt{s} [GeV]	model	function	R [fm]	λ	c
14.0	π ($\delta y=0.6$)	Gaussian	0.56 ± 0.02	0.46 ± 0.02	0.84 ± 0.00
		Exponential	0.72 ± 0.04	0.66 ± 0.02	0.83 ± 0.00
	ρ ($\delta y_\rho=1.2$) ($\delta y_\pi=0.6$)	Gaussian	0.77 ± 0.04	0.28 ± 0.01	0.85 ± 0.00
		Exponential	1.17 ± 0.09	0.43 ± 0.03	0.85 ± 0.00
34.5	π ($\delta y=0.8$)	Gaussian	0.50 ± 0.02	0.58 ± 0.02	0.90 ± 0.00
		Exponential	0.62 ± 0.02	0.83 ± 0.02	0.88 ± 0.00
	ρ ($\delta y_\rho=1.6$) ($\delta y_\pi=0.8$)	Gaussian	0.61 ± 0.02	0.39 ± 0.01	0.91 ± 0.00
		Exponential	0.80 ± 0.04	0.54 ± 0.02	0.91 ± 0.00
91.2	π ($\delta y=1.2$)	Gaussian	0.36 ± 0.01	0.62 ± 0.02	0.96 ± 0.01
		Exponential	0.42 ± 0.01	0.92 ± 0.01	0.91 ± 0.00
	ρ ($\delta y_\rho=2.4$) ($\delta y_\pi=1.2$)	Gaussian	0.48 ± 0.01	0.34 ± 0.01	0.96 ± 0.00
		Exponential	0.63 ± 0.02	0.49 ± 0.01	0.95 ± 0.00

Table III

\sqrt{s} [GeV]	R_L [fm]	λ_L [fm]	R_T [fm]	λ_T [fm]	τ [fm]	λ_τ
14.0	0.55 ± 0.03	0.32 ± 0.02	0.29 ± 0.16	0.07 ± 0.03	0.20 ± 0.00	0.20 ± 0.01
91.2	0.34 ± 0.01	0.34 ± 0.01	0.13 ± 0.05	0.04 ± 0.01	0.20 ± 0.01	0.13 ± 0.00

Table IV

\sqrt{s} [GeV]	a	b
14.0 ($\delta y=0.60$)	4.36	$0.054 \quad (0.085 \pm 0.014)$
34.5 ($\delta y=0.80$)	6.18	$0.074 \quad (0.089 \pm 0.003)$
91.2 ($\delta y=1.20$)	9.03	$0.137 \quad (0.118 \pm 0.009)$

Table V

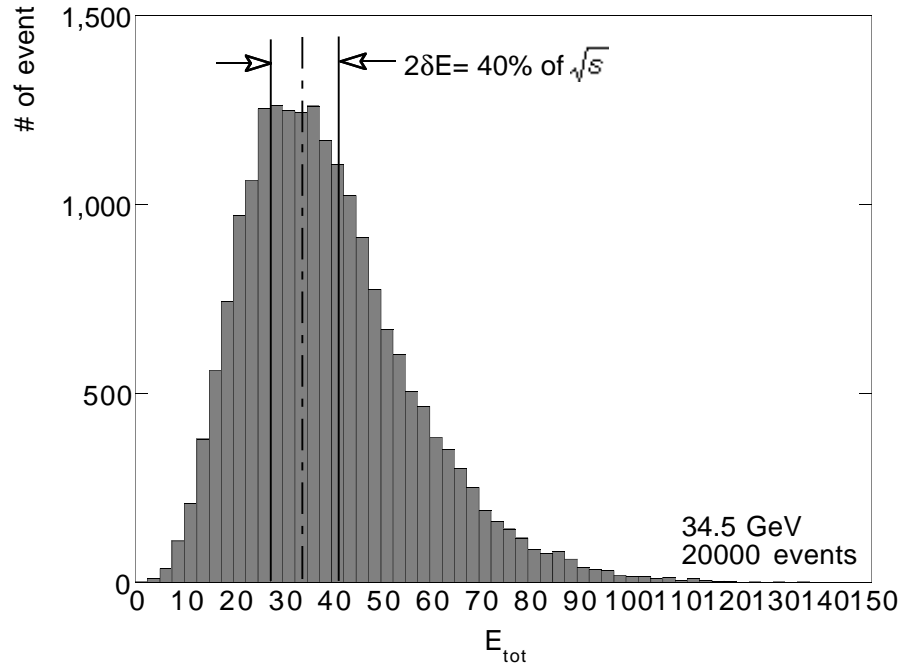


Fig.1

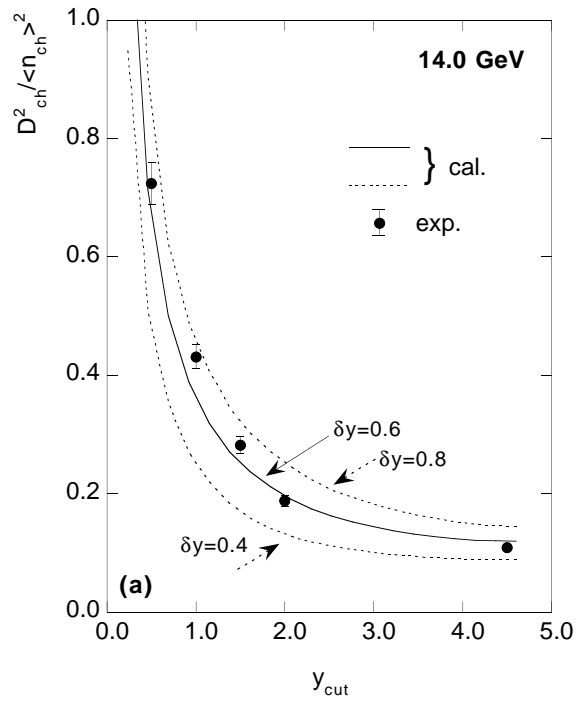


Fig.2

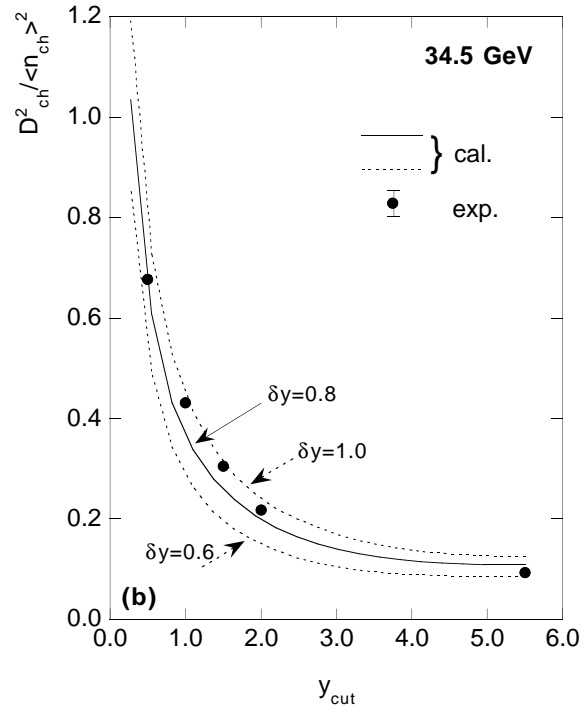


Fig.2

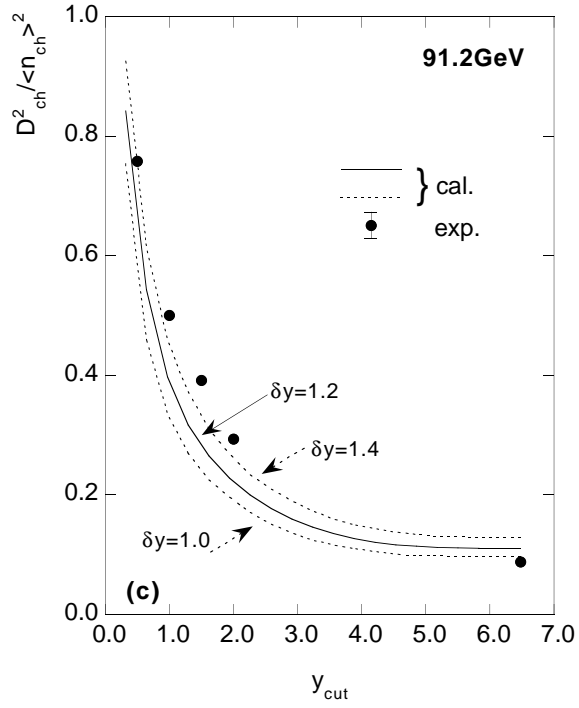


Fig.2

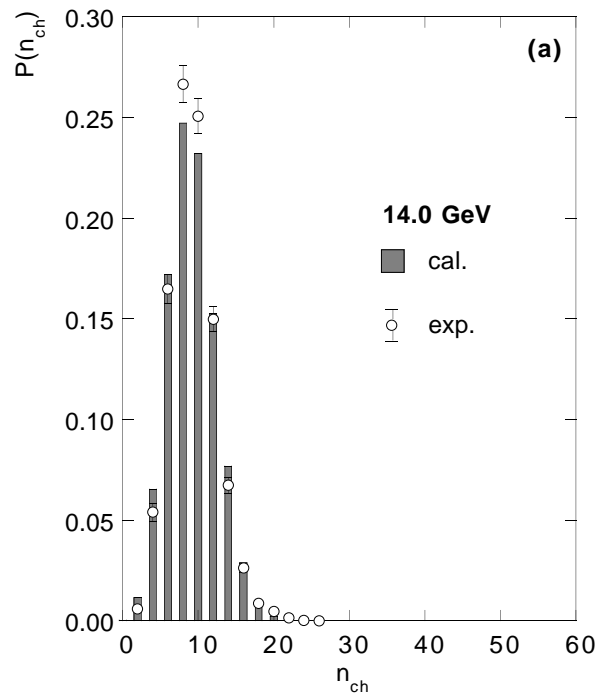


Fig.3

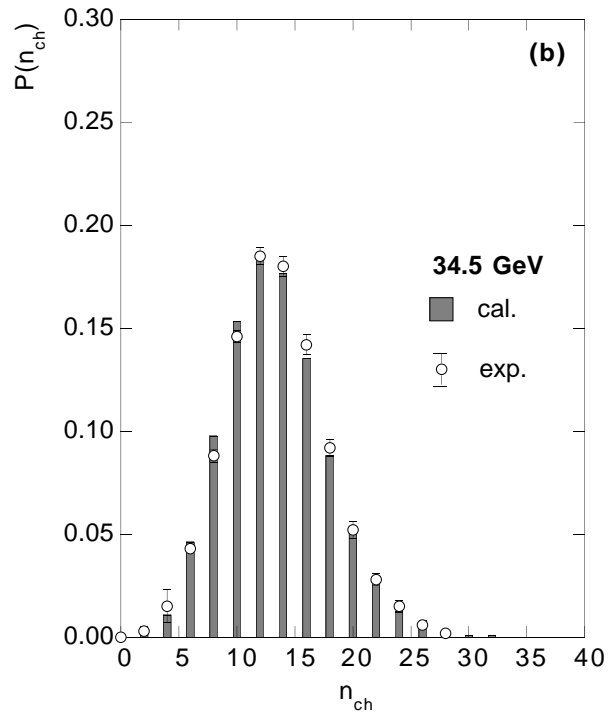


Fig.3

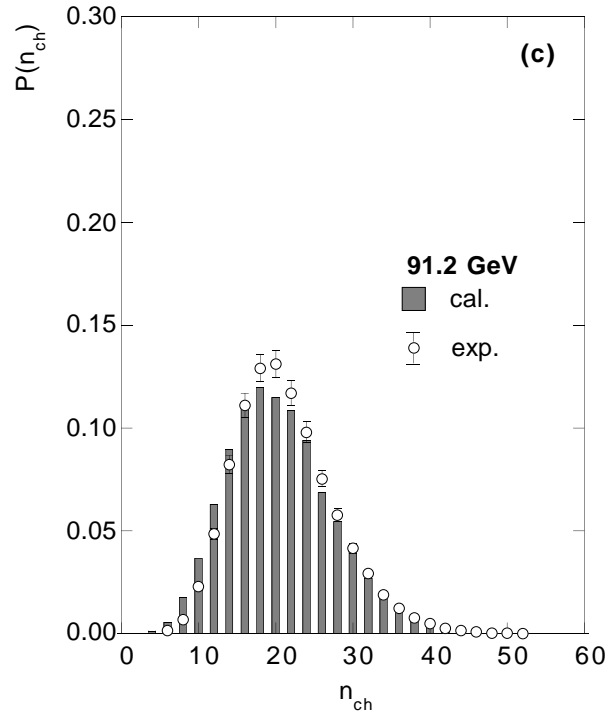


Fig.3

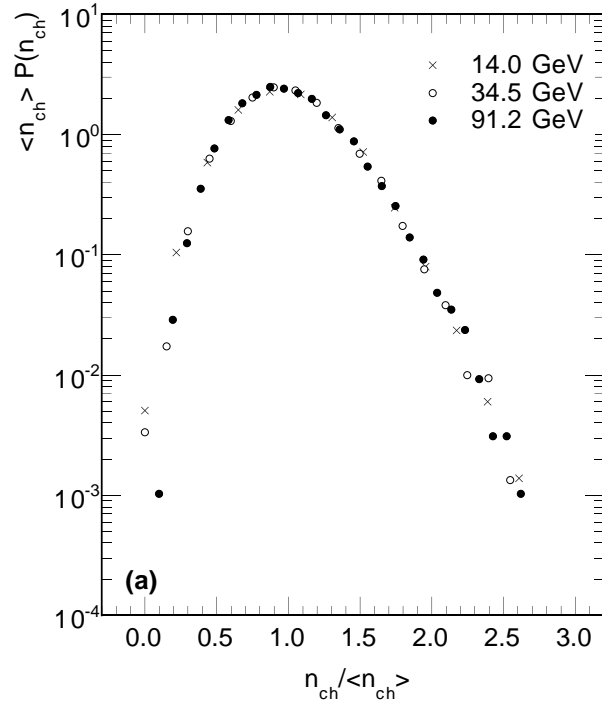


Fig.4

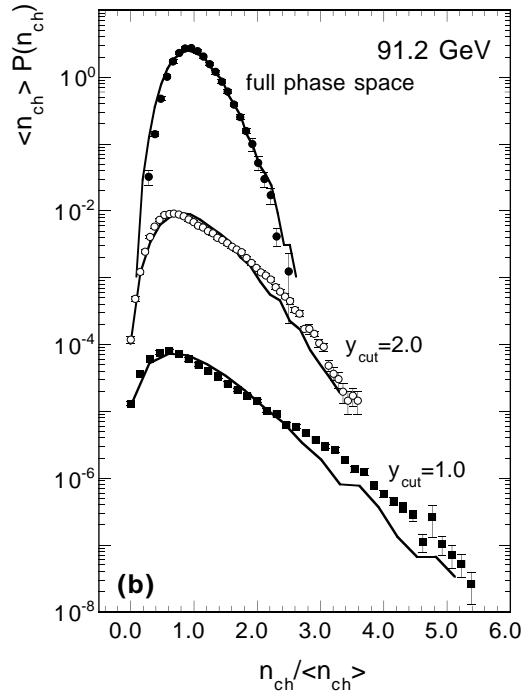


Fig.4

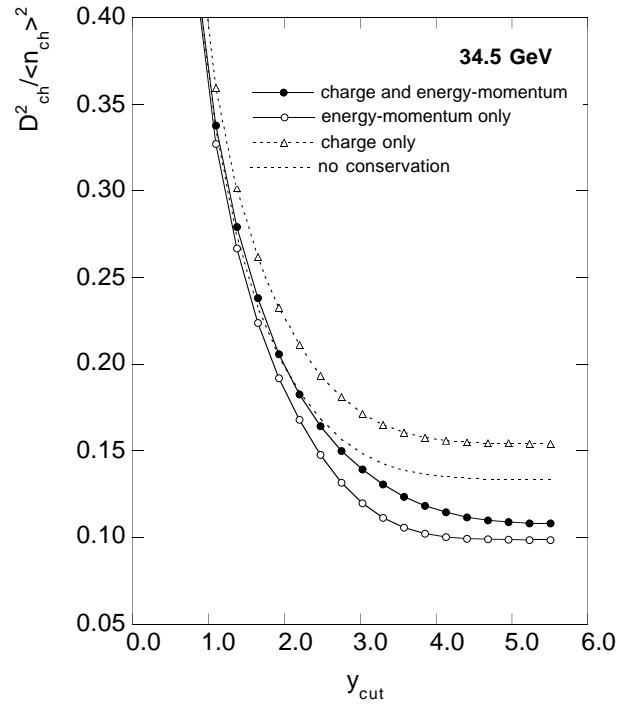


Fig.5

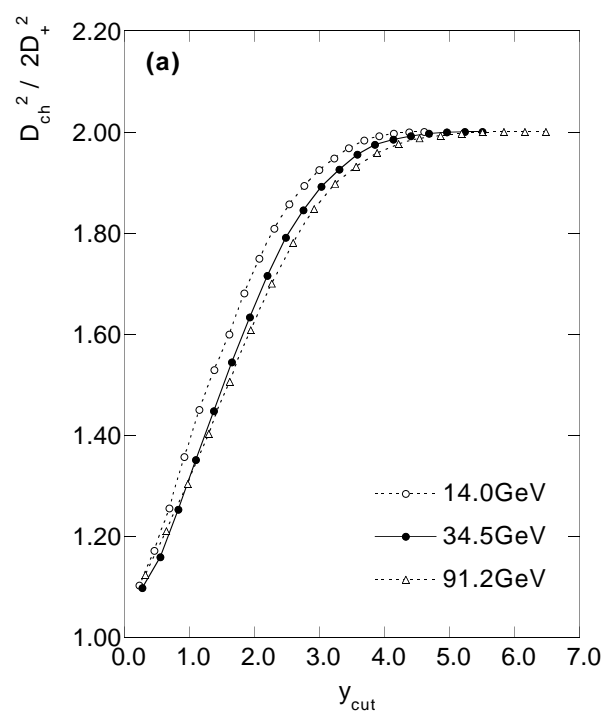


Fig.6

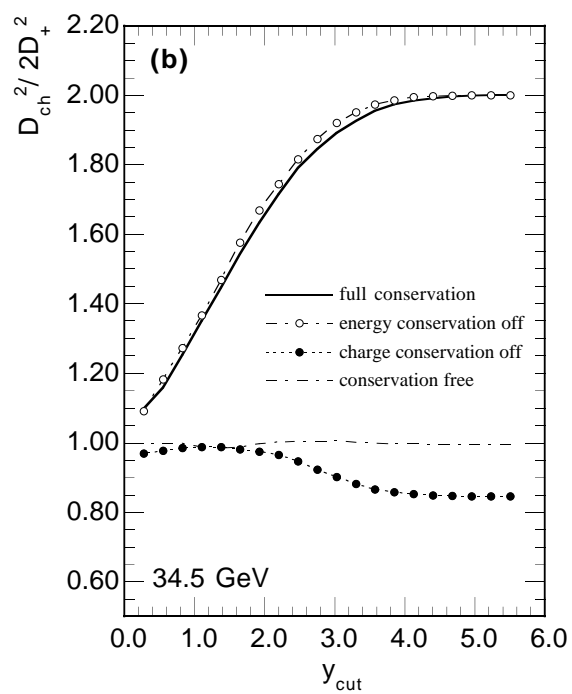


Fig.6

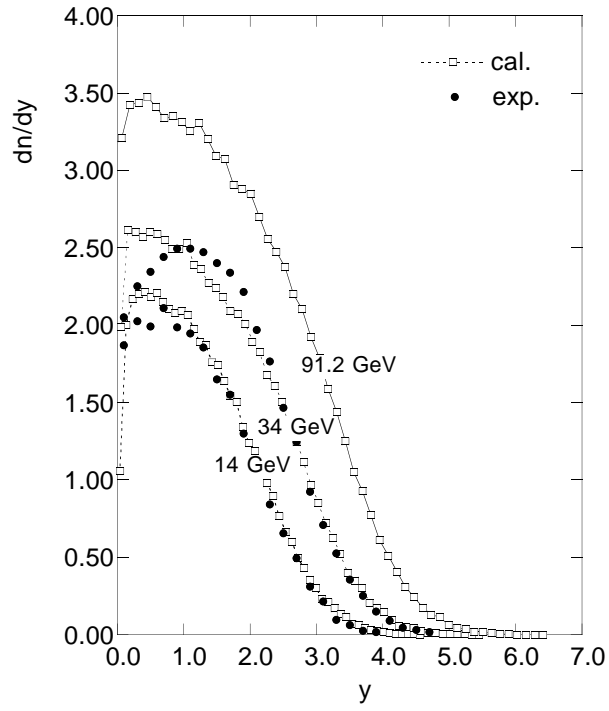


Fig.7

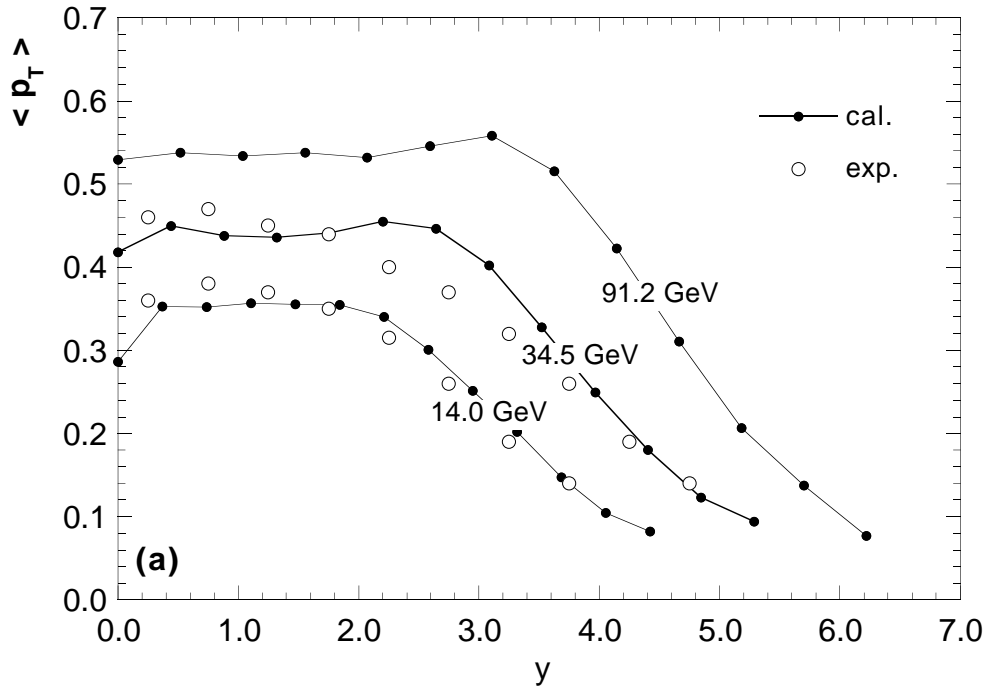


Fig.8

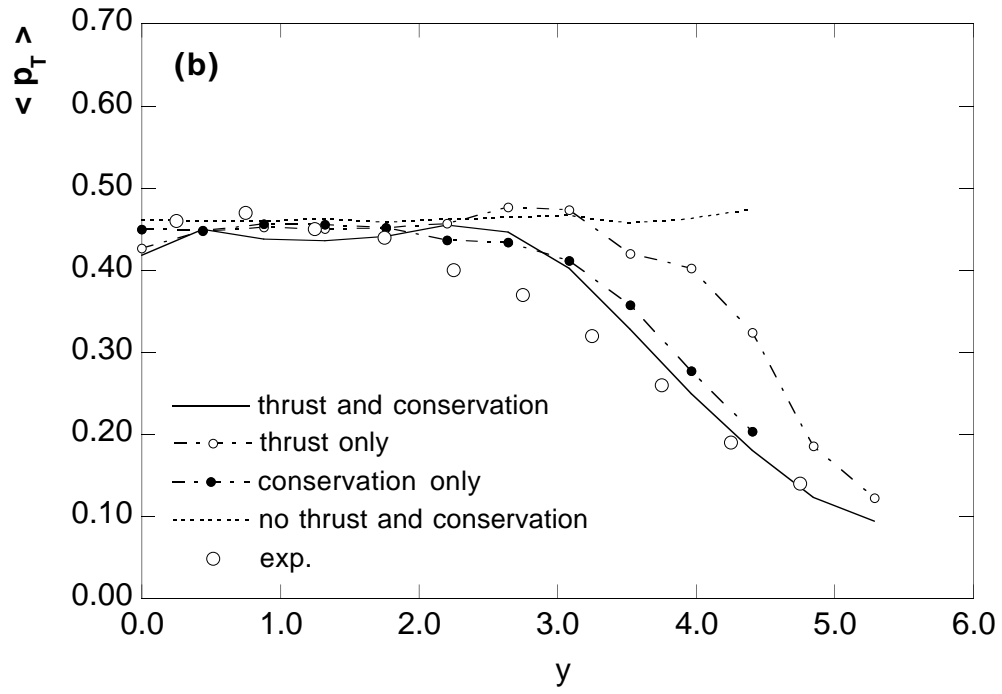


Fig.8

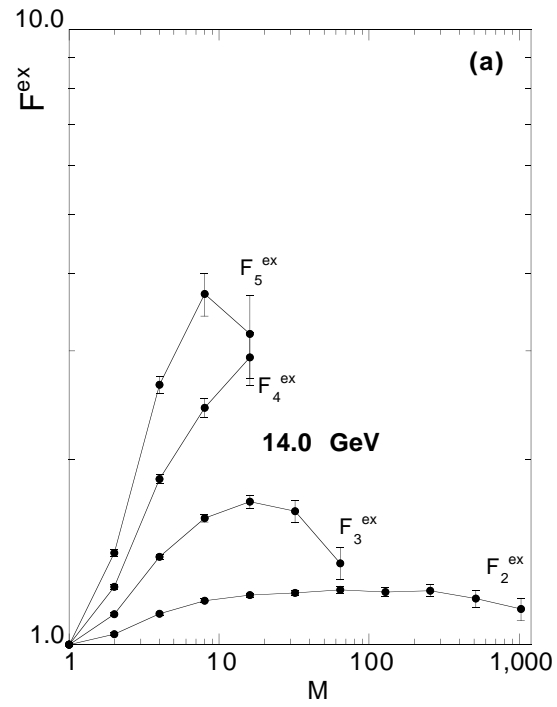


Fig.9

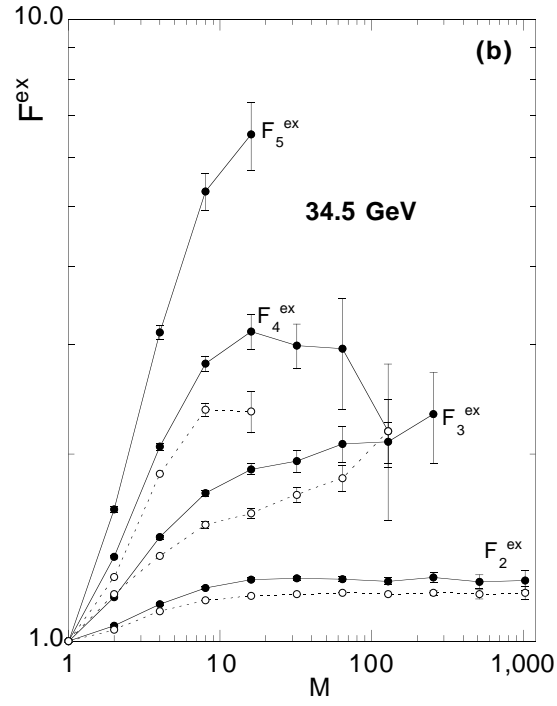


Fig.9

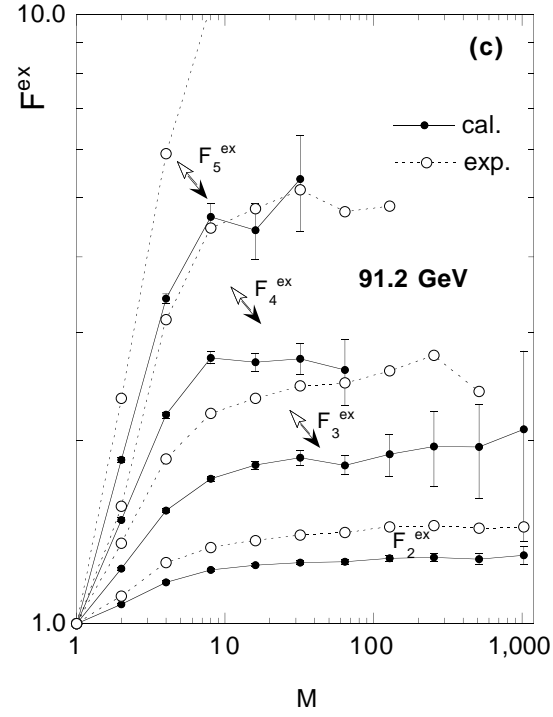


Fig.9

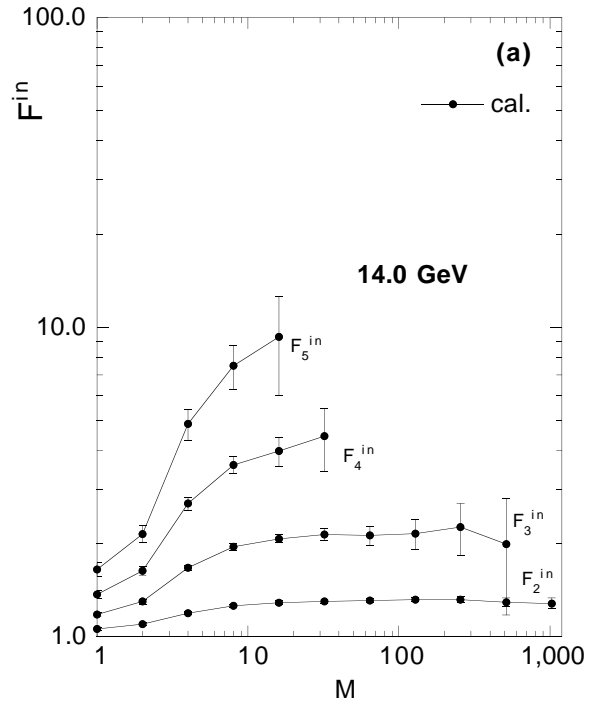


Fig.10

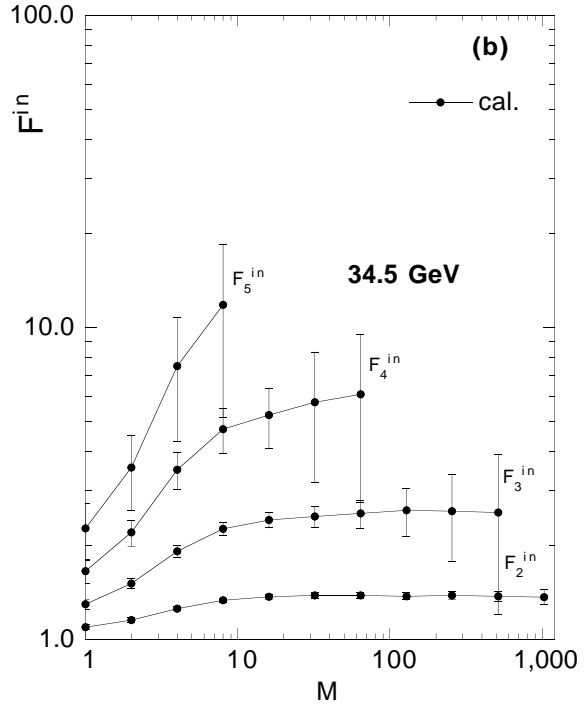


Fig.10

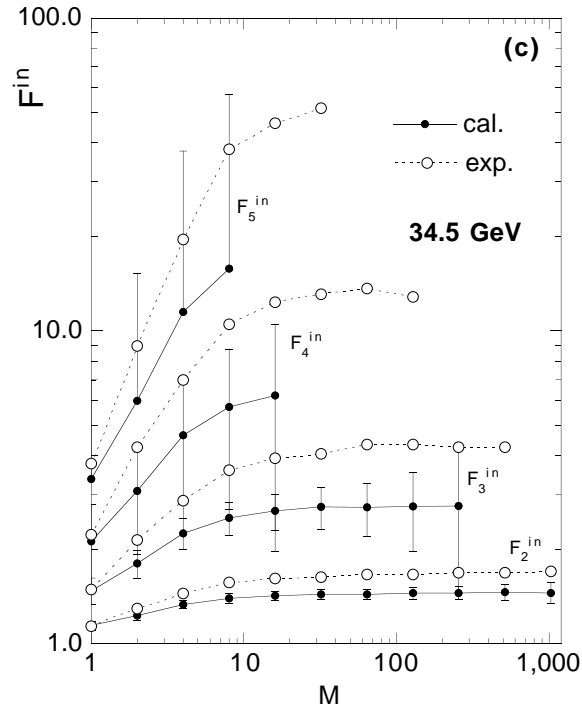


Fig.10

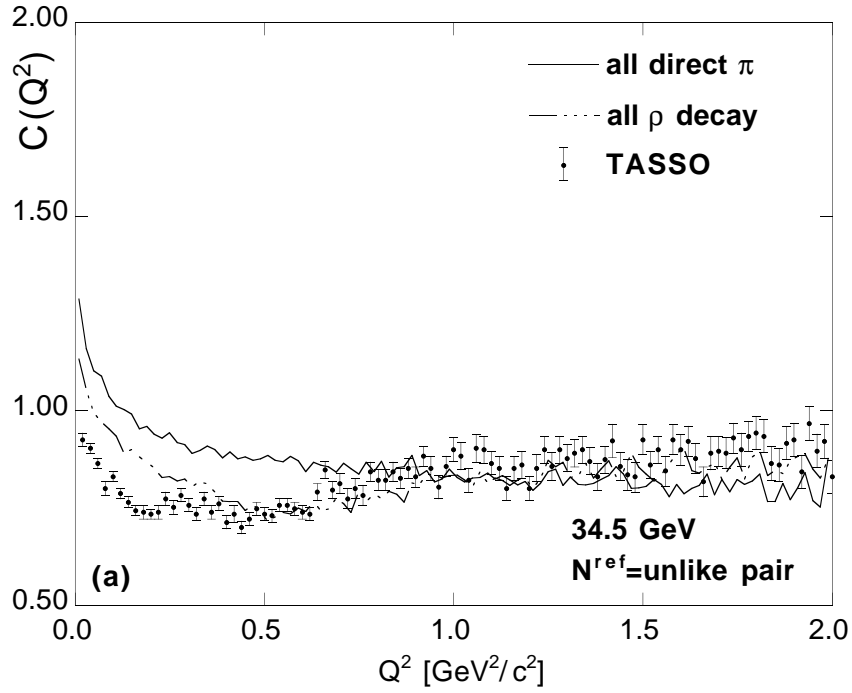


Fig.11

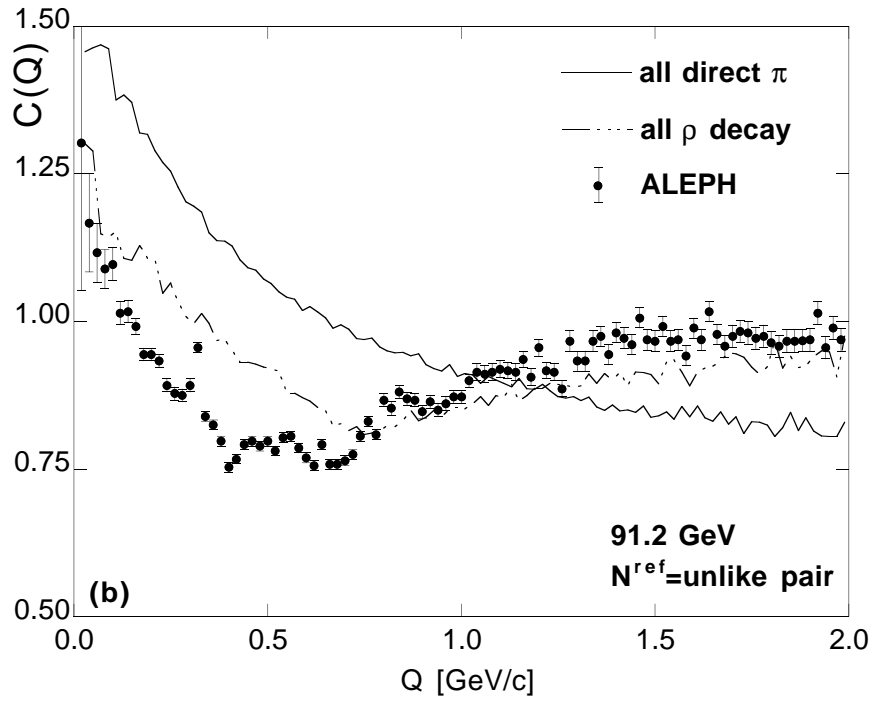


Fig.11

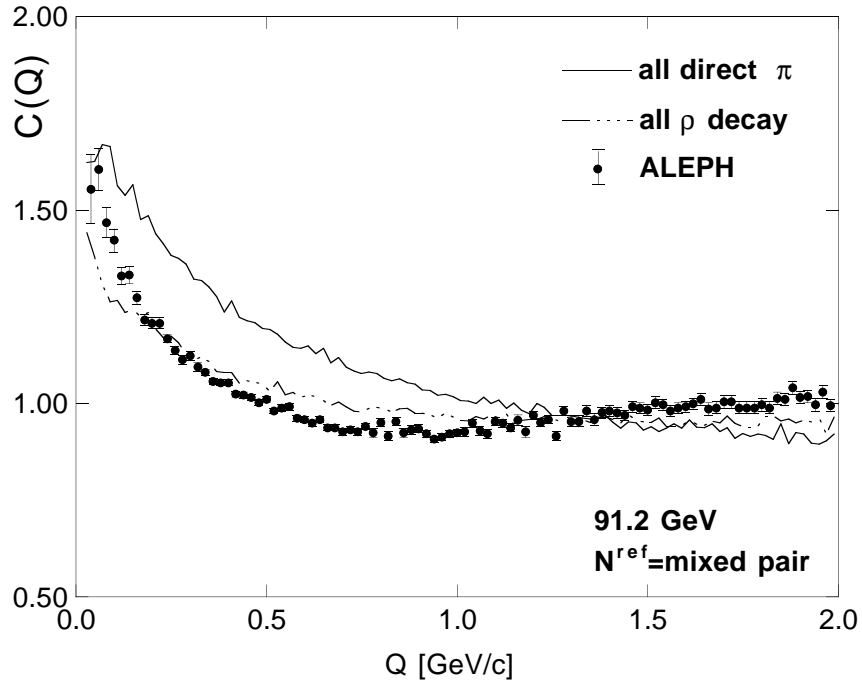


Fig. 12

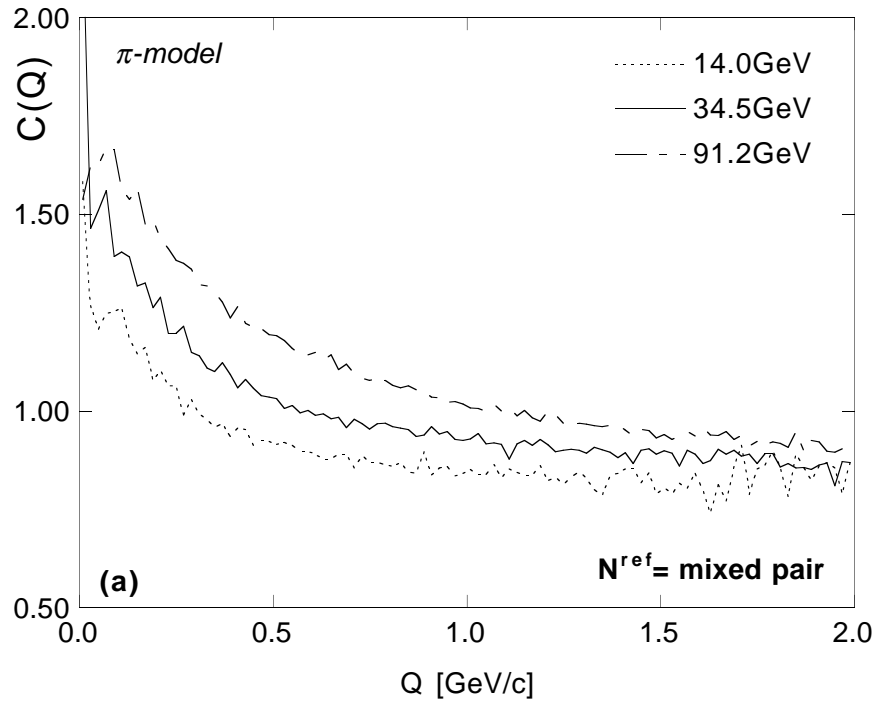


Fig.13

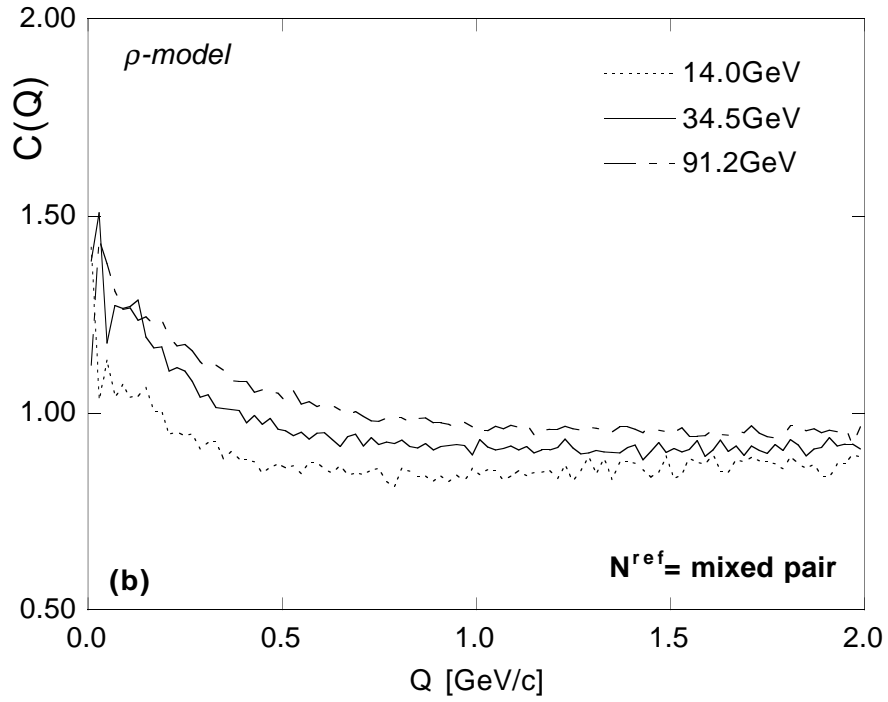


Fig.13

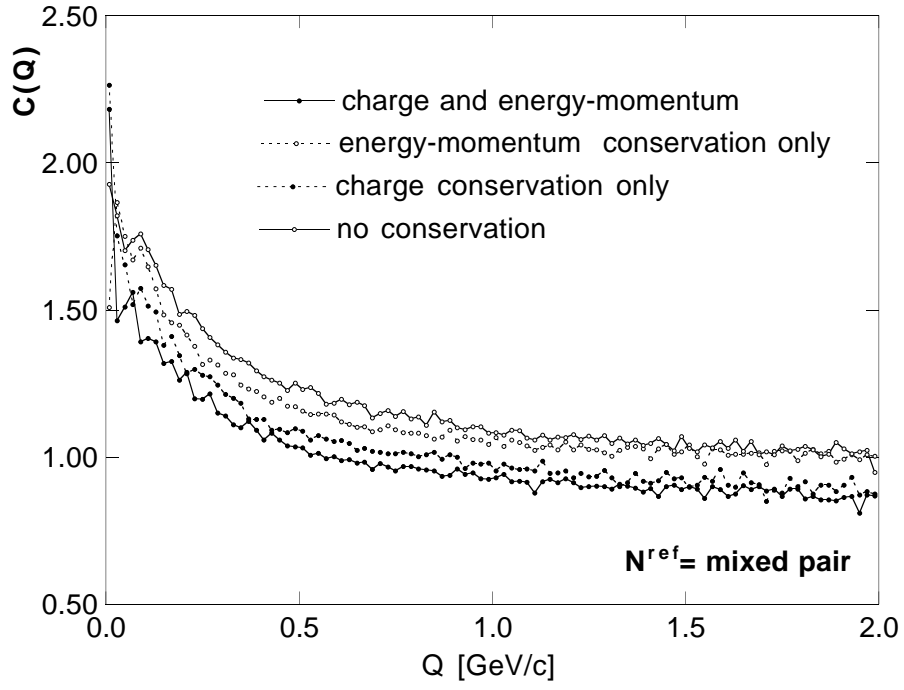


Fig.14

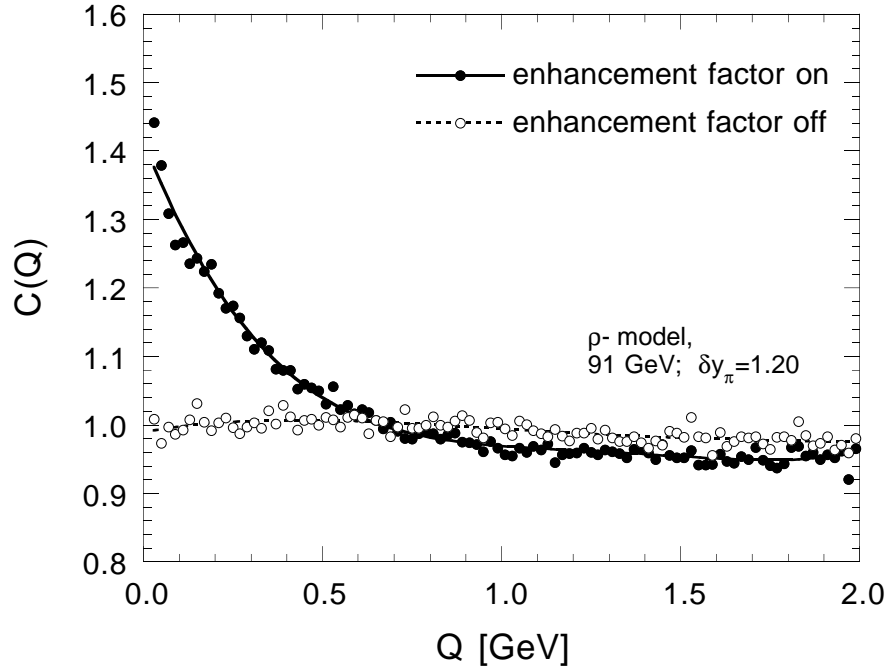


Fig.15

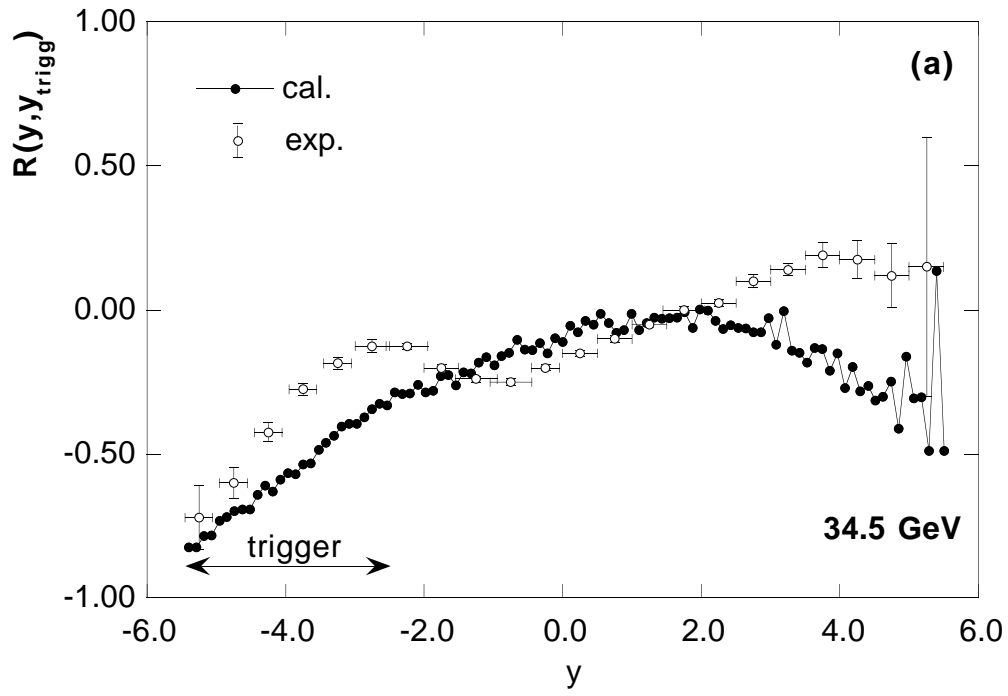


Fig.16

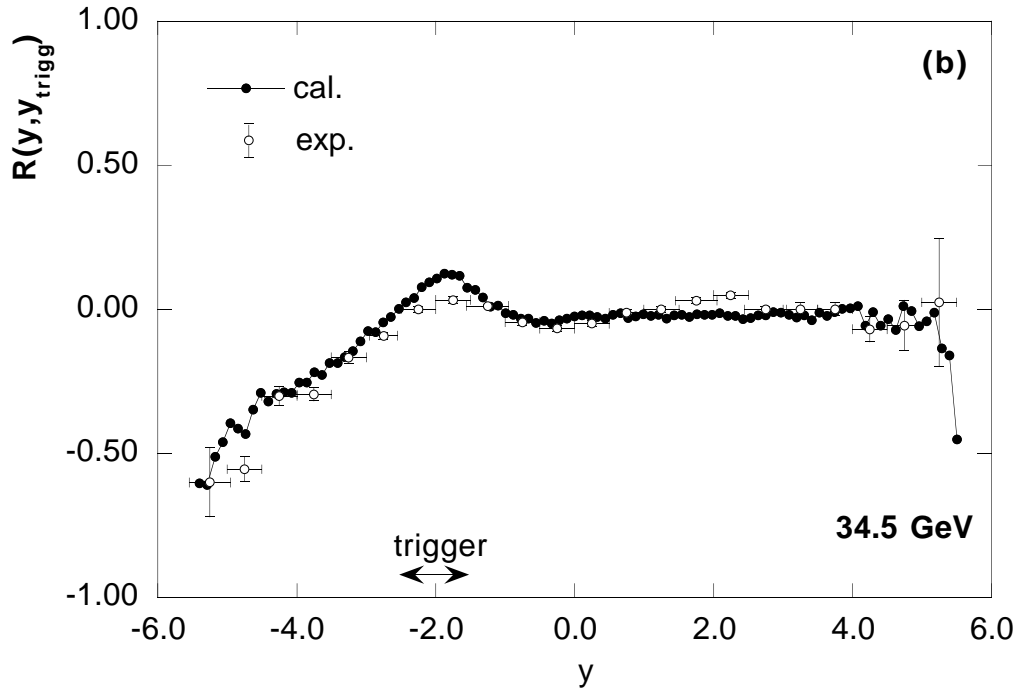


Fig.16

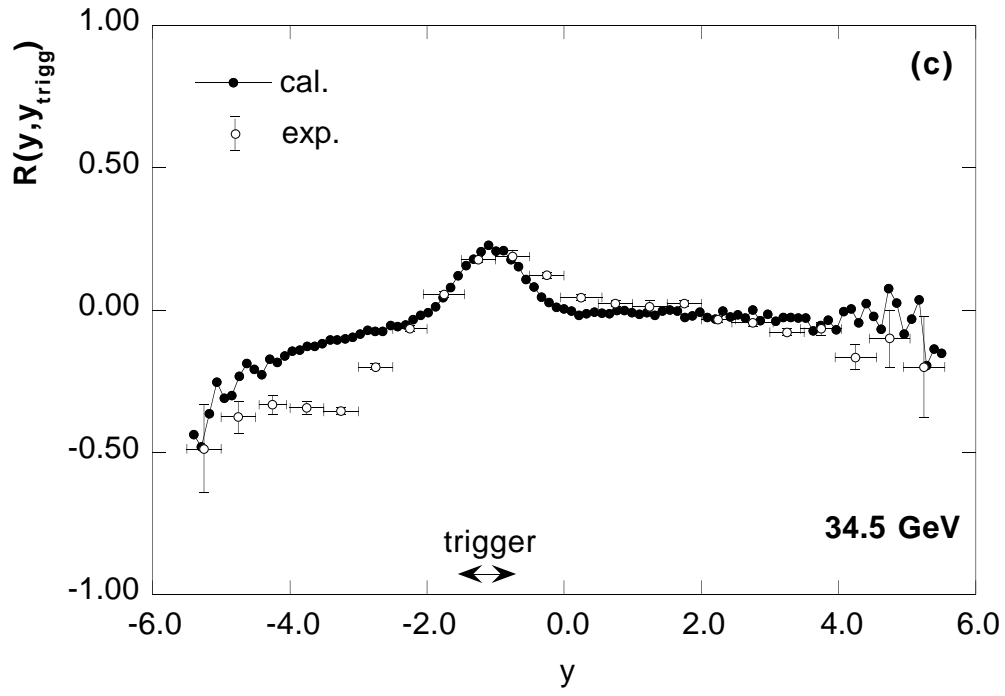


Fig.16

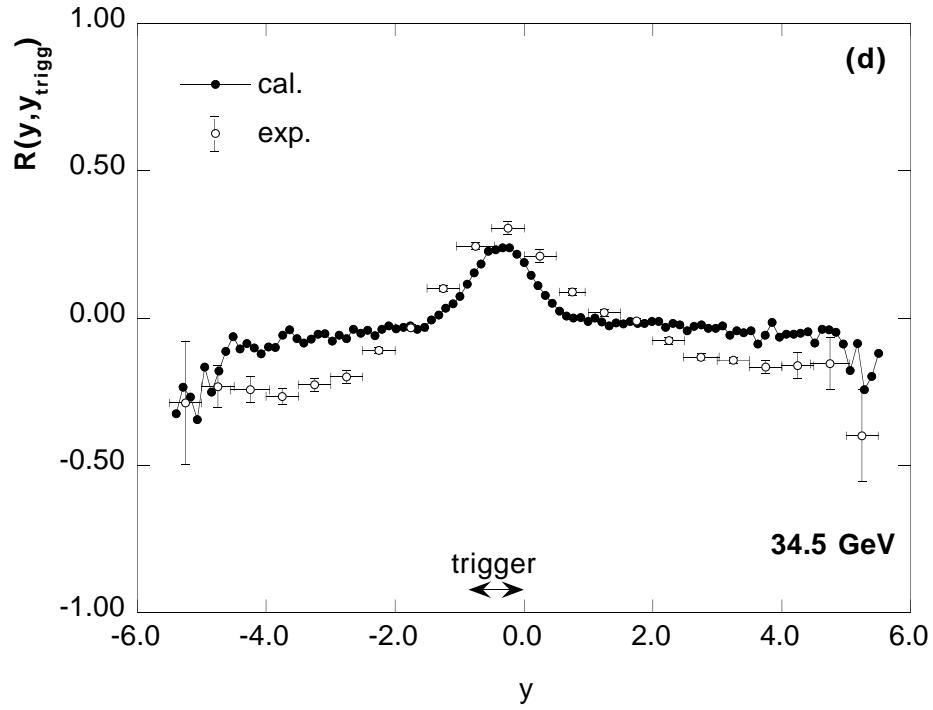


Fig.16

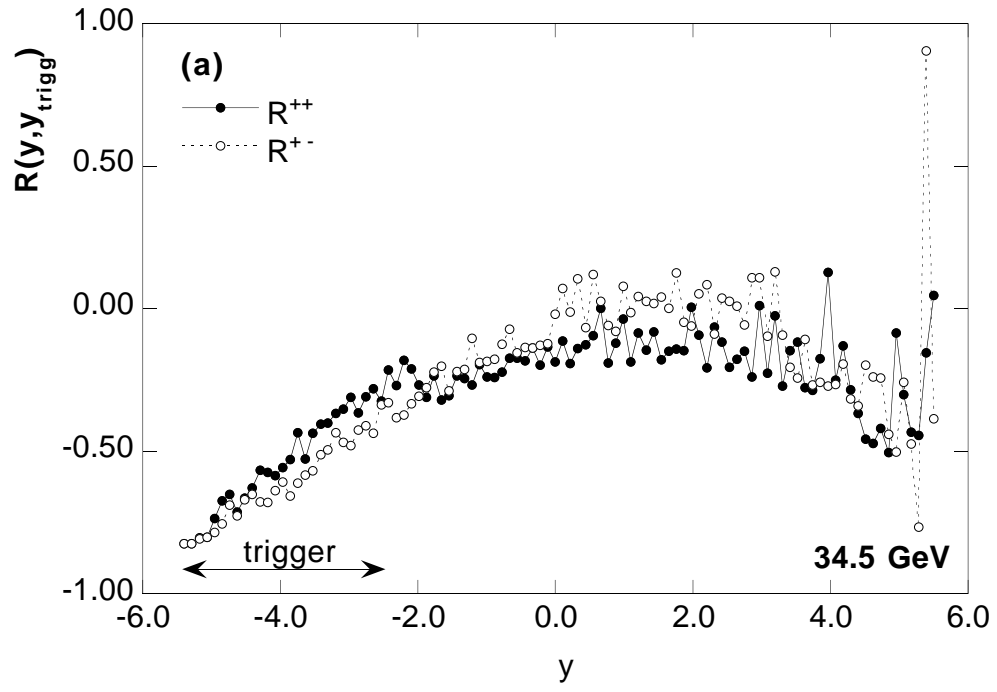


Fig.17

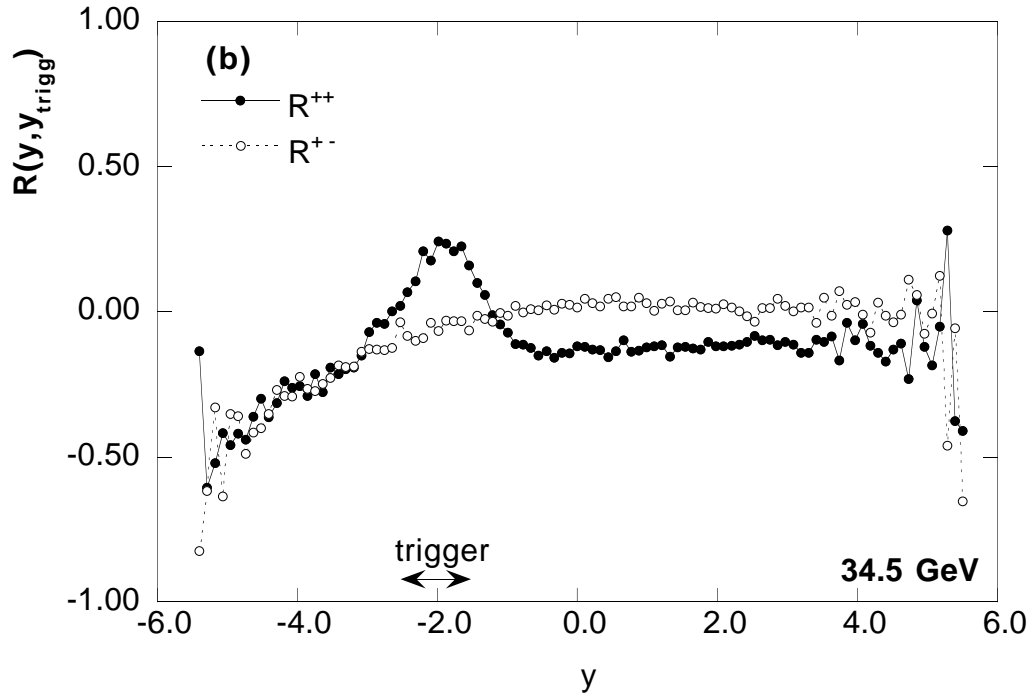


Fig.17

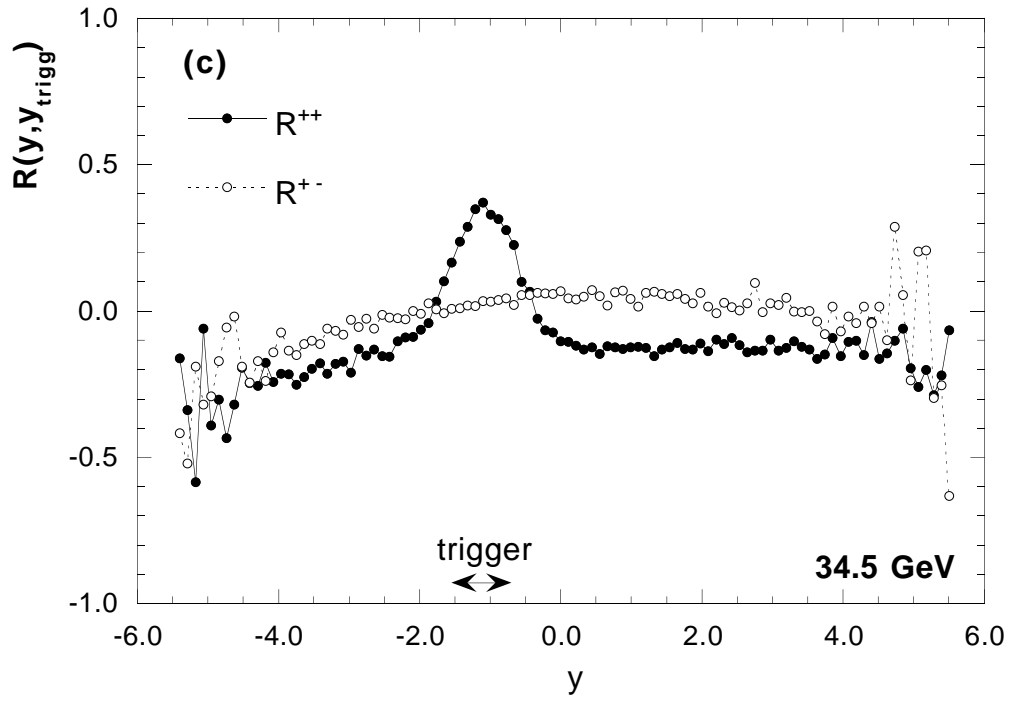


Fig.17

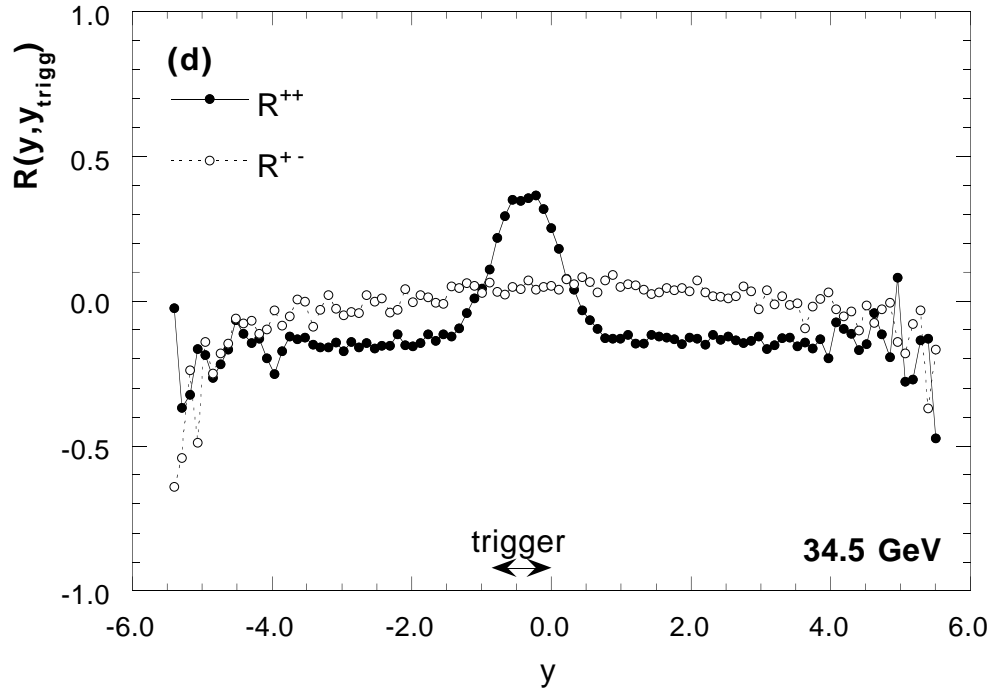


Fig.17

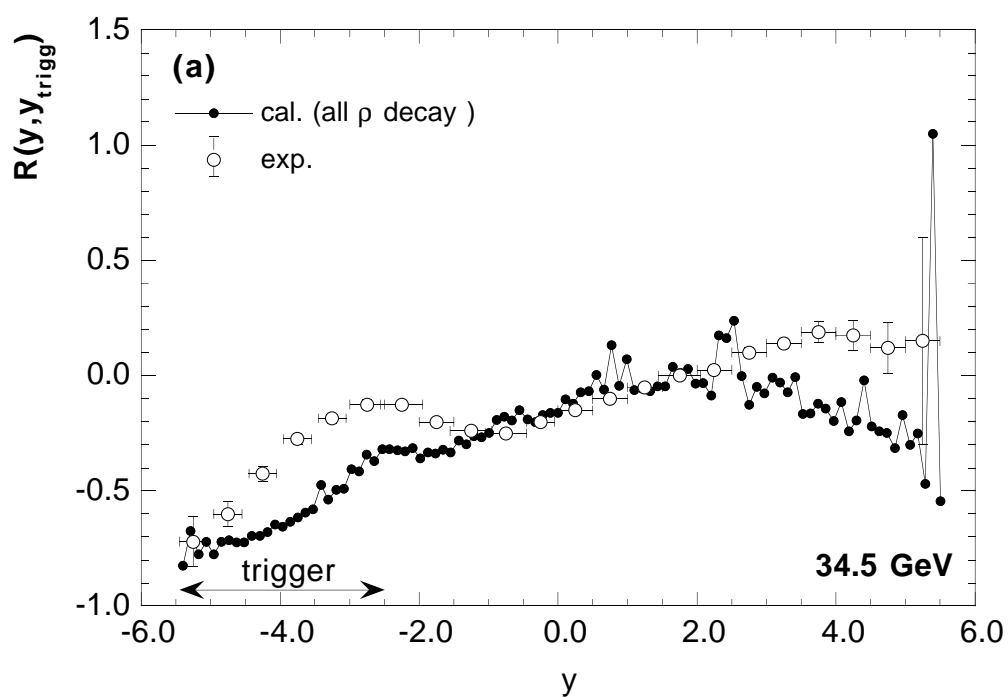


Fig.18

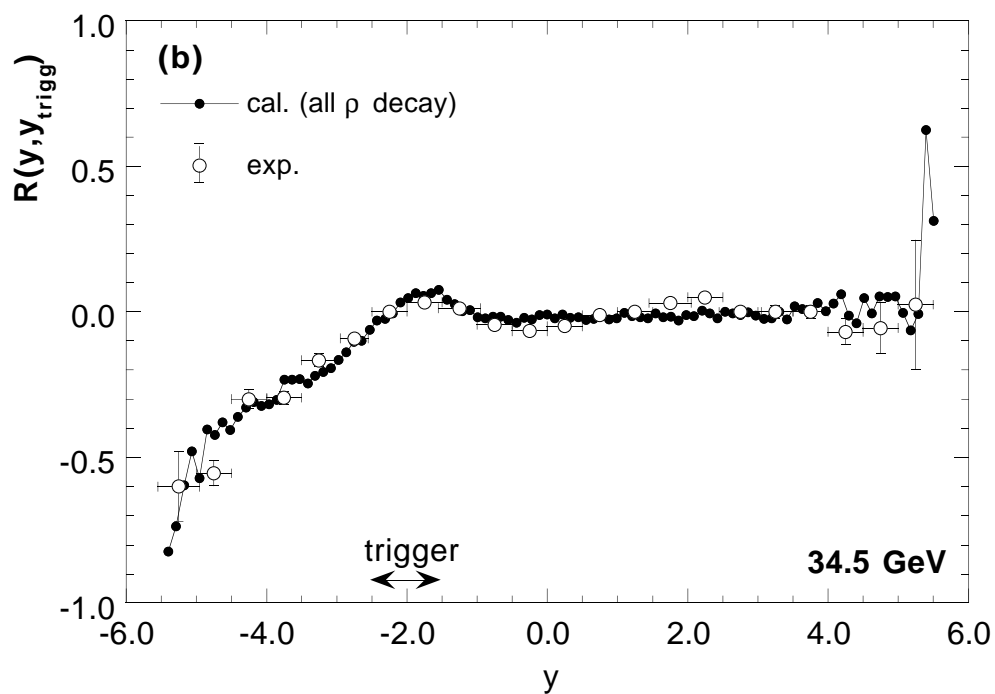


Fig.18

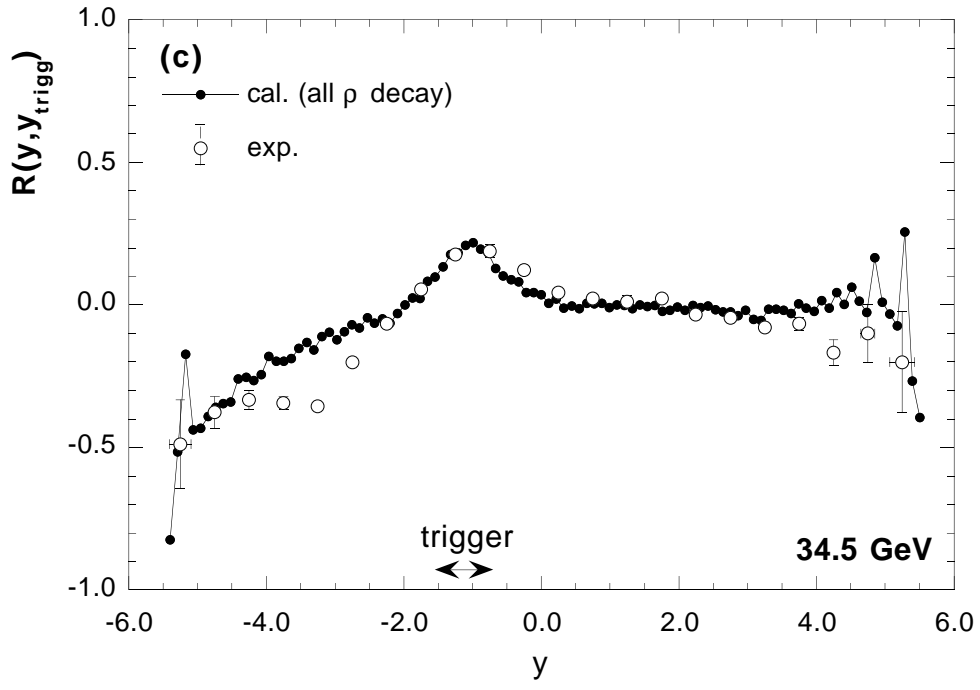


Fig.18

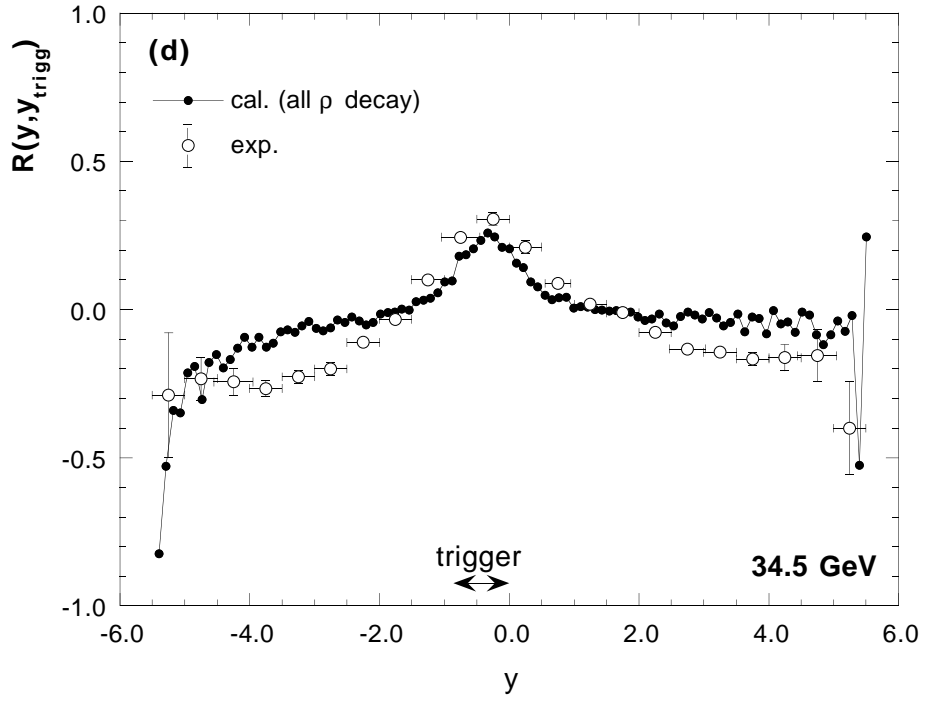


Fig.18

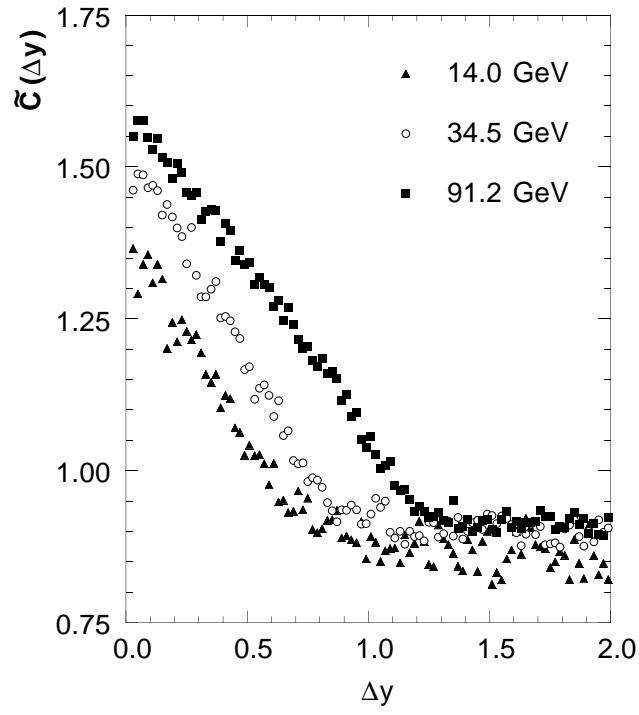


Fig.19

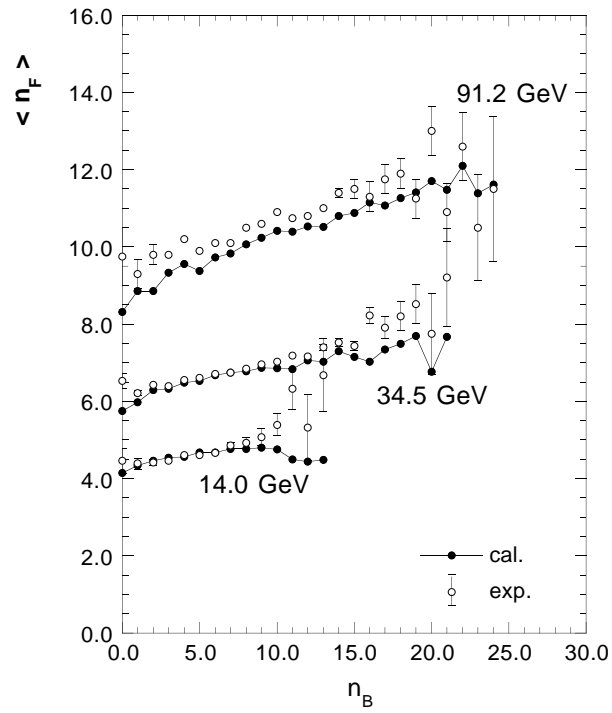


Fig.20